Chapter 12. Ship and Wake Detection

William G. Pichel
Office of Research and Applications, NOAA/NESDIS, Camp Springs, MD, USA

Pablo Clemente-Colón
Office of Research and Applications, NOAA/NESDIS, Camp Springs, MD, USA

Christopher C. Wackerman
General Dynamics - Advanced Information Systems, Ann Arbor, MI, USA

Karen S. Friedman
Office of Research and Applications, NOAA/NESDIS, Camp Springs, MD, USA

12.1 Introduction

Although not strictly an environmental measurement like the other parameters discussed in this manual, ship signatures are significant features frequently found in Synthetic Aperture Radar (SAR) ocean imagery. These signatures can provide information useful to environmental scientists, coastal and fishery managers, and law enforcement agencies.

Characteristics such as high resolution (10 to 100 m), sensitivity to small variations in surface roughness (on the order of centimeters), and especially the strong signal return from hard targets like ships make SAR systems particularly adept at detecting vessels at sea. Ships may be detected via three main mechanisms: (1) identification of radar energy reflected directly from the vessel, (2) detection of wake patterns, and (3) identification of slicks on the ocean surface resulting from release of engine or fish oils. Each mechanism is described and illustrated in this chapter, including the physical processes at work, important SAR image characteristics, and limitations inherent in today's satellite SAR systems. Finally, an example of a pre-operational ship-detection applications demonstration is presented.

12.2 Direct Detection of Ships

12.2.1 Physical Process

Spaceborne SAR instruments send out pulses of electromagnetic radiation and then measure the amplitude and phase of reflected radiation from the ocean, the land, or man-made objects (referred to as hard targets). Strong radar returns result from direct reflection from objects with high dielectric constant (i.e., conductors such as steel) oriented so that large surfaces are perpendicular to the incoming radar beam or arranged in angular corner-shaped structures (i.e., corner reflectors). Corner reflectors have the property of returning radiation back to the source, parallel to its incoming direction. Ships often contain superstructure or deck configurations that act as direct reflectors or corner reflectors. In addition, under the right orientation with respect to the radar beam, the hull and ocean together can, through a double reflection, return significant energy back to the satellite SAR antenna (see Figure 12.1).

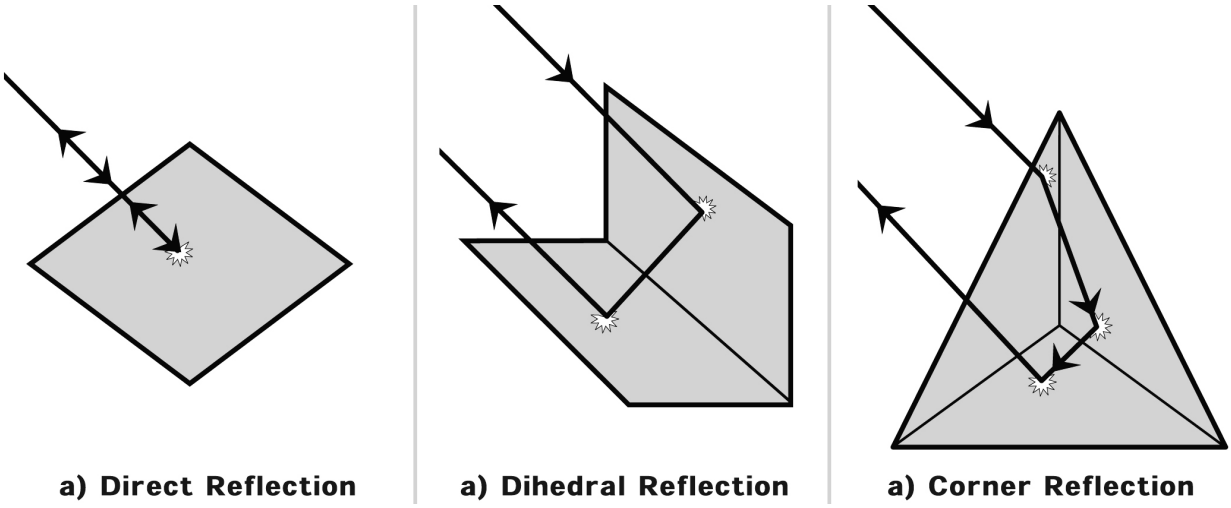

Figure 12.1 Radar pulses from a satellite can be reflected back to the detector by: (a) direct reflection, e.g. from portions of the ship perpendicular to the radar beam, (b) a double bounce off a dihedral reflector, e.g. the ocean and then the ship or vice versa, or (c) a corner reflection (triple bounce) e.g from the ship superstructure.

12.2.2 SAR Imaging Characteristics

The direct radar return from a ship is the most common ship signature in SAR imagery. Depending on the SAR resolution, the SAR image signature of a ship direct return may simply be a single pixel with significantly greater normalized radar cross section (i.e., large backscatter and therefore brighter) than surrounding pixels or, at higher resolution (e.g., 30 m or better), an elongated series of brighter pixels. At the highest resolutions (10 m or less), details of the ship superstructure may become distinguishable (see Figure 12.2c). As long as the ship has good radar backscatter characteristics, even ships smaller than the SAR pixel resolution can be easily detected under a fairly wide range of wind and wave conditions. The direct return from the ship is often the only ship signature, particularly (1) when the ship is not underway, (2) when higher winds or waves quickly destroy wake and slick signatures, or (3) when lower resolution modes, such as ScanSAR, are employed. Figure 12.2 is a collection of ship direct return signatures.

Automated ship detection algorithms generally look for a statistically significant contrast between the ship and the local ocean background. A single detection threshold cannot be used for the whole image since the background backscatter changes substantially with SAR angle of incidence, wind speed, and sea state. Various algorithm approaches have been developed which automatically adapt to changing background backscatter during the search for targets. Many of these algorithms are referred to as constant false alarm rate algorithms. Examples of ship detection algorithms can be found in *Eldhuset* [1996], *Vachon et al.,* [1997], and *Wackerman et al.,* [2001].

12.2.3 Limitations in SAR Detection

Limitations to the success of direct detection of ships with SAR systems can be grouped into the following five categories: (1) ship characteristics, (2) environmental conditions, (3) radar characteristics, (4) image quality, and (5) image resolution.

12.2.3.1. Ship characteristics. Ship characteristics, such as structural configuration, orientation with respect to the radar, ship size, and structural material have a highly significant

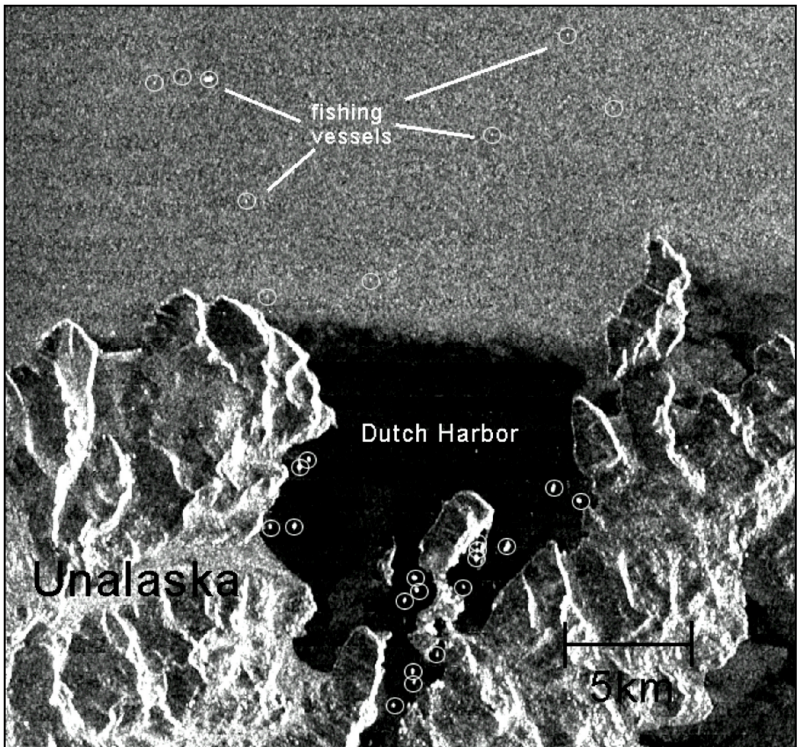

Figure 12.2a (left). RADARSAT-1 (C-band, HH) ScanSAR Wide B image acquired 20 February 1998 at 1729 UTC showing U.S. trawler fleet vessels (circled) anchored in Dutch Harbor, Alaska under very low wind conditions. Vessels are easy to detect since their large backscatter makes them stand out against the calm waters of the harbor. Outside the protection of the harbor where the wind is much higher, the ship/sea contrast is reduced. ©CSA 1998

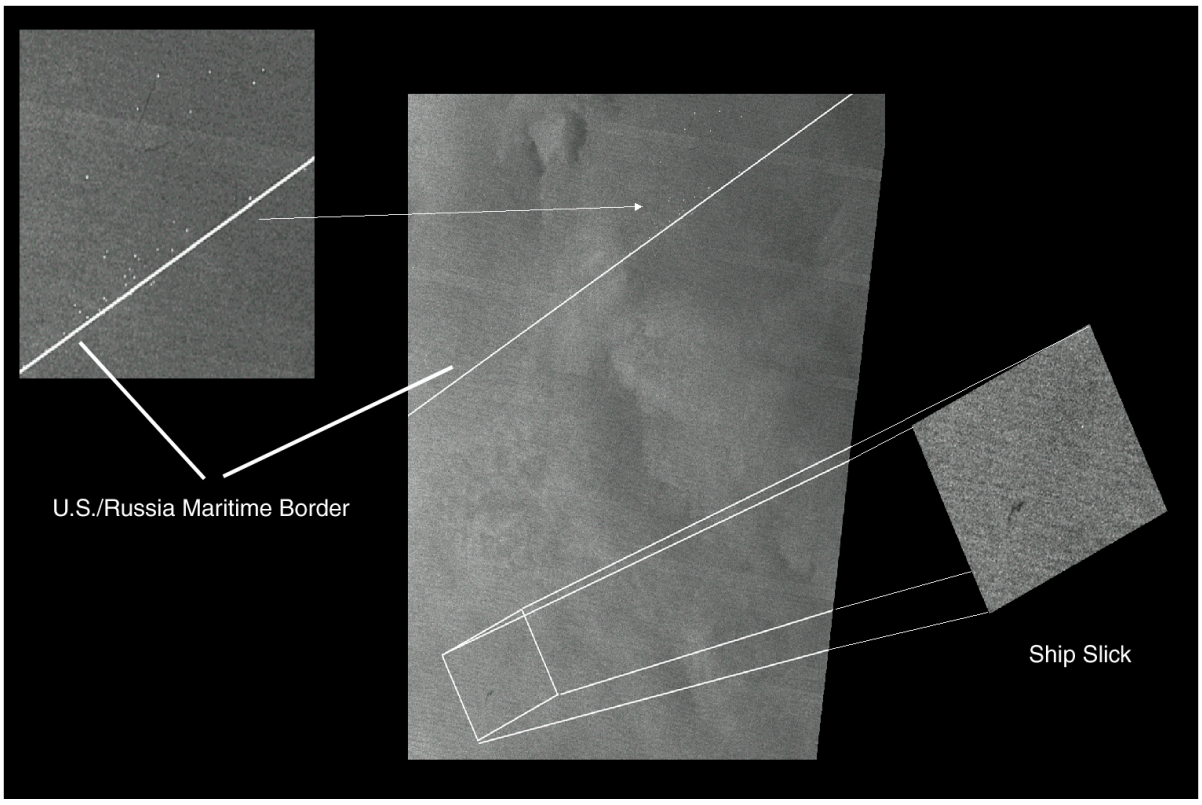

Figure 12.2b RADARSAT-1 (C-band, HH) ScanSAR Wide B image acquired 30 July 2000 at 1809 UTC showing the Russian walleye pollack trawler fleet lined up along the U.S./Russia maritime border. The U.S. Coast Guard seized a Russian trawler 800 yards inside the U.S. Exclusive Economic Zone on the U.S. side of the maritime border on 1 August 2000 in this area of the border. ©CSA 2000

Figure 12.2c RADARSAT-1 (C-band, HH) Standard Mode image of a large ship showing some ship structure. Image was acquired on 5 November 1997 at 1111 UTC. The ship is located off the east coast of the U.S. near Chesapeake Bay. ©CSA 1997.

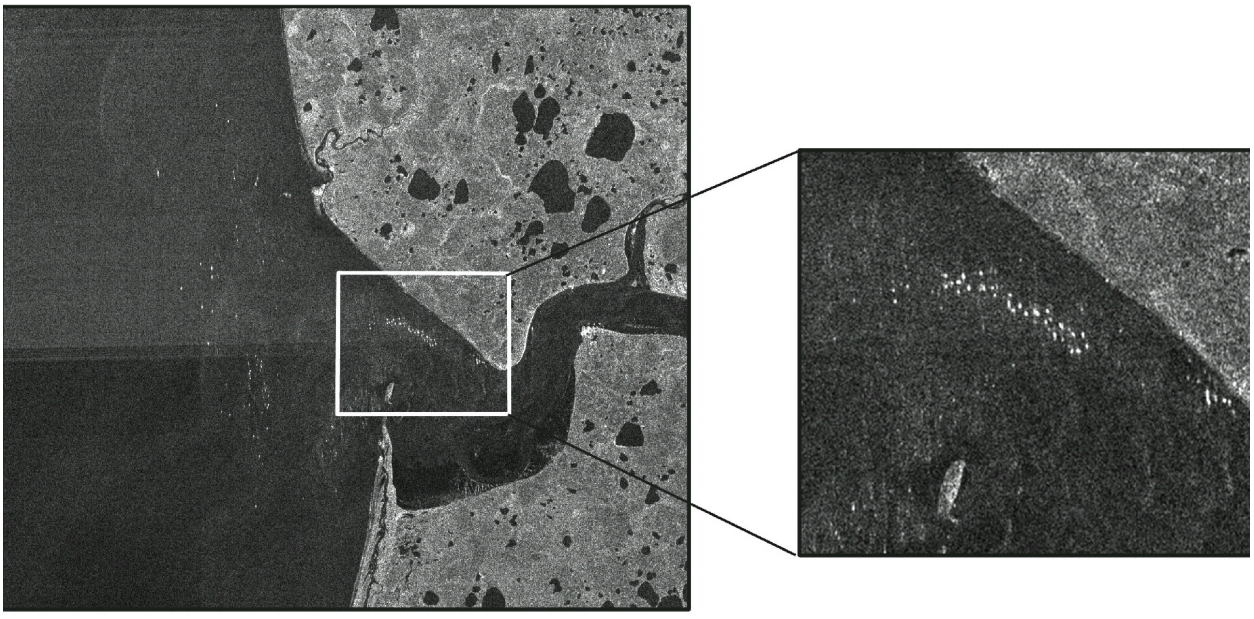

Figure 12.2d. RADARSAT-1 (C-band, HH) Standard Mode image acquired 5 July 2004 at 0411 UTC showing small fishing vessels (approximately 10 m in length in the Egegik Bay salmon fishery in Bristol Bay, Alaska (58.2N, 157.5W). ©CSA 2004

effect on the ability of SAR systems to detect a particular vessel. A ship made from materials with high dielectric constant (i.e., from materials that are good electrical conductors such as steel) is a better radar reflector than a vessel made of non-conducting materials such as fiberglass or wood. A vessel with substantial superstructure consisting of natural corner reflectors is a particularly good target. Also, a ship traveling perpendicular to the radar beam (i.e., traveling in the same direction as the satellite is flying - generally north or south) presents as a larger target and has the possibility of a greater double reflection return.

12.2.3.2. Environmental conditions. Environmental characteristics, such as sea state, wind speed, proximity to land, and presence of ice affect the ability to distinguish SAR ship signatures from the ocean background return. The greater the wind speed or the higher the waves, the greater the environmental contribution to the radar return signal, and thus the weaker the contrast between the vessel and the ocean background (see Figure 12.2a). Ships are detected under wind conditions ranging from no wind up to somewhat over 10 m s^{-1} [*Vachon et al*., 2000 found a validated vessel where the wind speed was 13.2 m s^{-1}]. In coastal regions, it is hard to distinguish between a ship and a small island without intimate knowledge of the near-shore geography. And along the ice edge, SAR signatures of ship-sized pieces of ice are often indistinguishable from those of vessels fishing or traveling nearby.

12.2.3.3 Radar characteristics. Characteristics of the radar instrument, such as angle of incidence (i.e., the angle between a line connecting the radar with the reflecting surface being viewed and the local normal to the surface), polarization, resolution, and sensitivity affect the ability to detect vessels with a SAR system. The radar signal return from the ocean's surface is a function of angle of incidence, with the return falling off as the angle of incidence increases. A ship return, however, does not change as dramatically with angle of incidence; thus, at higher angles of incidence there is improved contrast between the ship and the ocean background (Figure 12.3). In general, RADARSAT-1 Standard Mode HH polarization imagery provide more contrast between ships and the background ocean than ERS-1/2 Standard Mode VV polarization imagery since VV imagery exhibit greater ocean return at a given angle of incidence than does HH imagery. However, more information on wake structures is provided by VV imagery. Recent research indicates that use of multipolarization SAR data (e.g., from the ENVISAT Advanced SAR and eventually from the ALOS Phased Array L-band SAR and the RADARSAT-2 SAR) may allow improvements in discrimination between ships and ocean clutter [*Touzi et al*., 2001; *Yeremy et al*., 2002].

12.2.3.4. Image quality. SAR image processing errors and the inherent speckle noise in SAR imagery can interfere with vessel detection algorithms. Speckle is noise in the image manifesting as random pixels that are much brighter or darker than the average of surrounding pixels. The speckle noise is a result of constructive or destructive interference during the coherent addition (i.e., taking account of phase as well as amplitude) of backscatter from many different scatterers within a resolution cell of the SAR image during the image integration time (i.e., for all the SAR pulses that illuminate a resolution cell as the satellite passes over). Speckle noise in low-backscatter regions of an image where the surface return is below the noise floor (i.e., the minimum detectable SAR backscatter) of the SAR instrument can appear as small vessels to a ship-detection algorithm. The speckle noise of a SAR image will also ultimately limit the minimum vessel size that can be detected, since smaller vessels will become

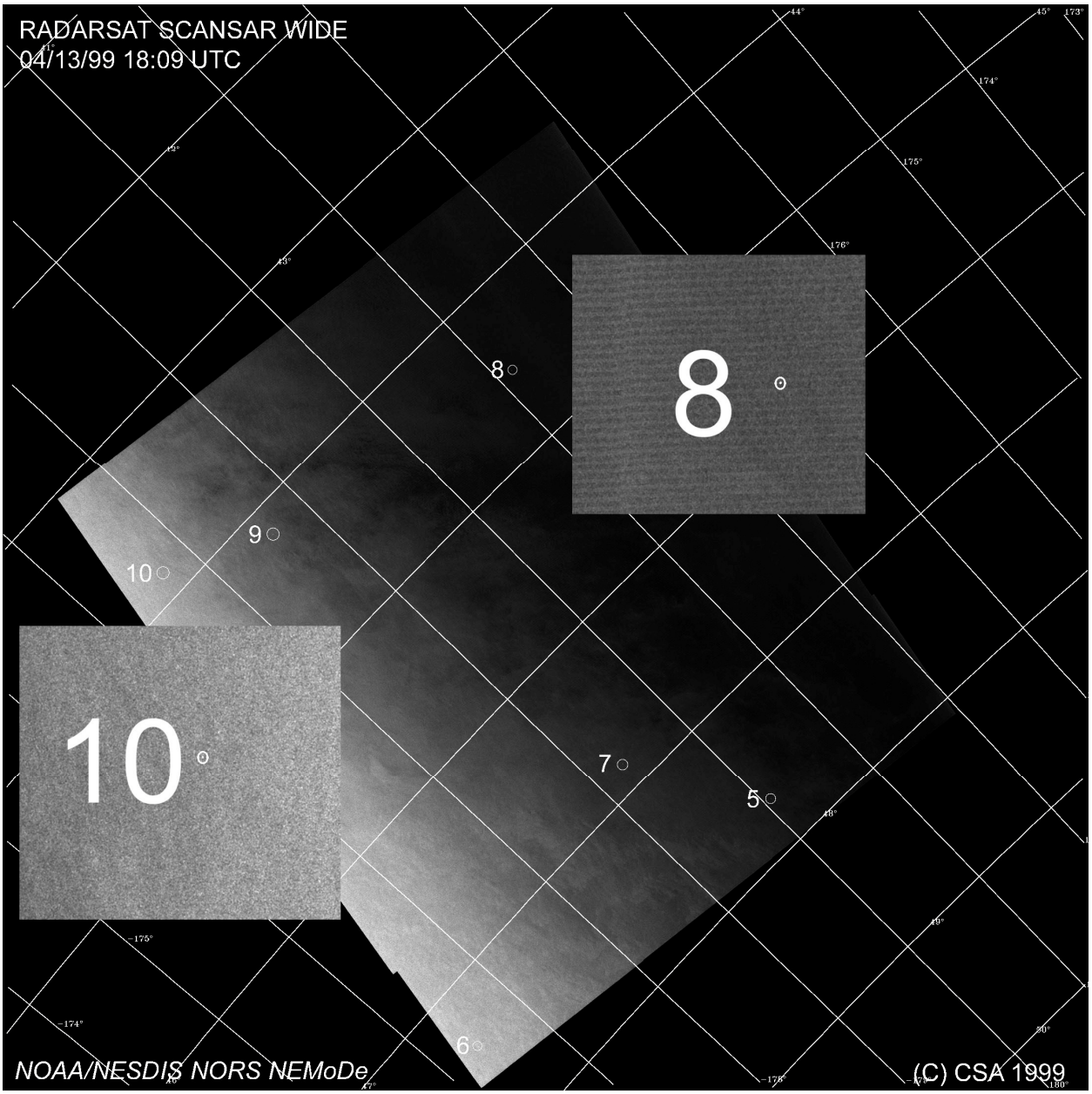

Figure 12.3. This 500 km RADARSAT-1 (C-band, HH) ScanSAR Wide B image acquired 13 April 1999 at 1809 UTC in the North Pacific exhibits a large contrast between ship signatures and the ocean background at high angles of incidence (right side of image Target 8). At smaller angles of incidence (left side of image - Target 10) the background ocean return increases and the ship-ocean contrast decreases. ©CSA 1999

indistinguishable from speckle. Processing problems such as obvious seam boundaries between beams in ScanSAR imagery, nadir ambiguities (an along-track bright line resulting from the timing of the direct return from the earth immediately below the satellite), scalloping in ScanSAR imagery (a cyclic banding pattern caused by errors in Doppler processing), and cross-track noise lines caused by processing errors can all be problematic—mainly by masking hard targets within erroneous high backscatter anomalies. It should be noted that these processing problems are, for the most part, processor dependent; i.e., for the same SAR signal data, different

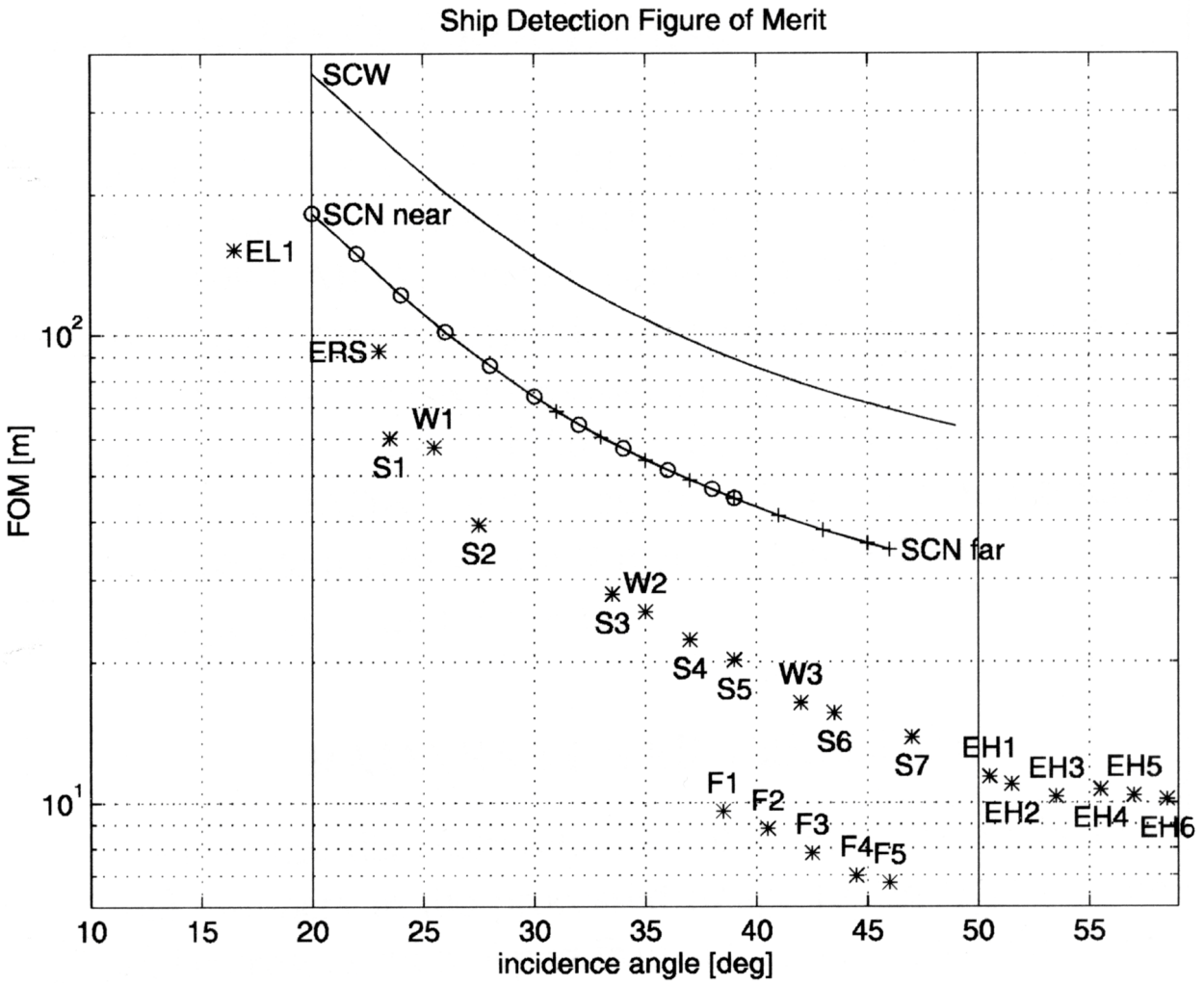

Figure 12.4. Plot of the ship detection Figure of Merit for the beam modes of RADARSAT-1 as a function of SAR angle of incidence [after *Vachon et al.,* 1997]. Figure of Merit (FOM) is defined as the minimum detectable ship length for a wind speed of 10 m s^{-1}, with wind blowing in a direction toward the radar. Graphs shown are for RADARSAT-1 ScanSAR Wide (SCW) and ScanSAR Narrow (SCN) Near and Far Beam Modes. Points are for various single beam modes: Standard (S), Wide (W), Fine (F), Extended High (EH), Extended Low (EL) of RADARSAT-1 and for ERS-1/2 (ERS).

SAR processors will produce slightly different SAR images when attempting to handle difficulties encountered during processing. Finally, image earth location errors can interfere with the correct discrimination between small coastal islands and coastal vessels.

12.2.3.5. Image Resolution. Although all the different modes (with their specific resolution and swath width characteristics) of available satellite SAR imagery are useful for detection of ships, particularly larger ships, some modes are better than others. *Vachon and Olsen* [1998] recommend for RADARSAT-1 that ship surveillance (i.e., when the approximate location is not known) be done with ScanSAR Narrow far-range imagery (50 m resolution, 300 km swath with angles of incidence between 31° and 46°) or ScanSAR Wide imagery (100 m resolution, 450-510 km swath with angles of incidence from 20° to 49° - see Figure 12.2b). Tracking (i.e., when the area of operation of the ships are known approximately) can be done

more effectively with higher resolution modes (Standard, Wide, or Fine Beam - see Figure 12.2d). The ScanSAR beams provide greater area coverage but are not useful for detecting small coastal fishing boats.

Figure 12.4 [*Vachon et al.,* 1997] shows the relative utility for ship detection of all the RADARSAT-1 beam modes and ERS-1/2 imagery. The angle of incidence (or range of angles) for each beam is indicated along with a Figure of Merit (FOM) for ship detection. The FOM is defined as the minimum detectable ship length for a wind speed of 10 m s^{-1}, with wind blowing in a direction toward the radar (i.e., the case resulting in the highest ocean clutter and thus the worst ship detection conditions). Considerably smaller ships will be seen for lower wind speeds or other wind directions. This figure clearly shows the performance of each SAR mode relative to all the other modes when employed for vessel detection. Also, one can see that for a particular type of beam as the angle of incidence increases, smaller and smaller vessels are detectable.

In a test of the ship detection algorithm used in the Alaska SAR Demonstration (see Section 12.6 below), *Friedman et al.,* [2000] found that between 45% (for 200 m resolution data) and 60% (for 100 m resolution data) of the vessels participating in the Bristol Bay Alaska red king crab fishery were detected in RADARSAT-1 ScanSAR Wide imagery. It is estimated that the detected ships were all longer than 33.5 m. *Vachon et al.,* [2000] obtained a detection rate (for ships averaging 120m) of 84% overall and 97% using the higher resolution modes of RADARSAT-1 that are recommended for ship detection. Ship detection performance improved as wind decreased, angle of incidence increased, and resolution increased.

12.3 Wakes

The track left in the water by a moving vessel, the wake, is an important clue in the detection of ships. Wake structures fall into four categories: (1) turbulent wakes stretched out directly behind the vessel, (2) the Kelvin wake formed by decameter-scale surface gravity waves generated by the passage of the vessel and propagating outward from the vessel track, (3) narrow-V wakes visible through Bragg scattering from short centimeter-scale waves generated by hydrodynamic processes along the ship's hull, and (4) internal wave wakes generated under conditions of shallow stratification [*Lyden et al.,* 1988; *Shemdin,* 1990]. Figure 12.5 illustrates the geometry of these different wake categories. Each category will be discussed below in terms of physical processes, SAR image characteristics and limitations in today's SAR systems.

12.3.1 Turbulent Wakes

Turbulence formed by breaking waves, water disturbed by the ship’s hull, and the action of the ship’s screws all disturb and then dampen the small-scale waves directly behind a passing vessel. Immediately behind the ship is a region of foamy, turbulent water followed by a much longer region of smooth water [*Peltzer, et al.,* 1987]. This is called the turbulent wake (see Figure 12.5b). Rising plumes of bubbles bring surface-active materials from within the water column and concentrate them at the surface, enhancing small-scale wave suppression. Damping of small waves in the turbulent wake is a result of increased viscosity, decreased temperature, and changes in surface tension and elasticity in the surface skin of the ocean [*Peltzer et al.,* 1992].

After the direct radar return from the ship itself, the most common ship-related signature in SAR imagery is the turbulent wake. This type of wake appears in imagery as a dark line

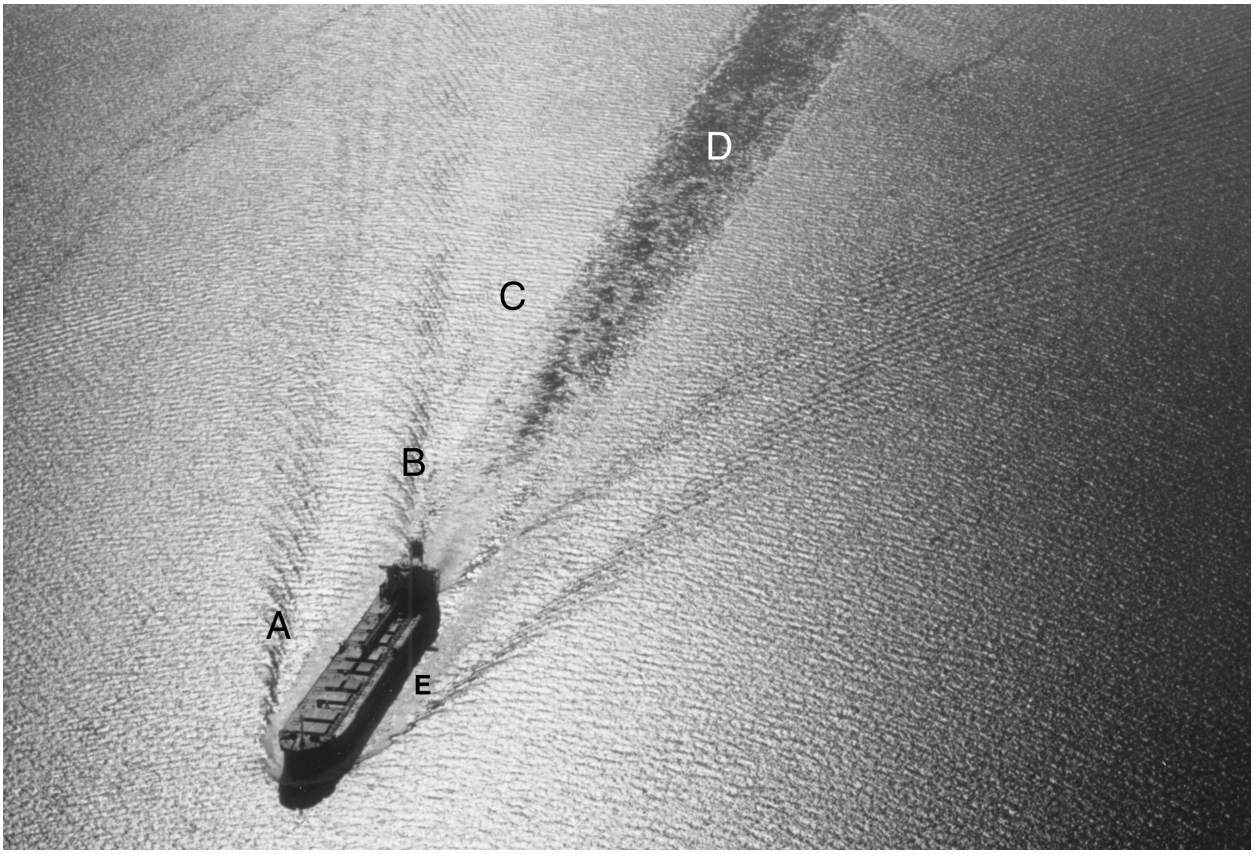

Figure 12.5a. Oblique 35 mm photograph of ship and its wake in Chesapeake Bay acquired 20 November 1999 near Annapolis, Maryland, showing a classic Kelvin "V" wake and a turbulent wake. Photo by author taken from plane piloted by Ronald Pichel. Figure 12.5c diagrams the components of the ship wake labeled in the photograph: A) bow wave, B) stern wave, C) transverse wave, D) turbulent wake, and E) turbulence region adjacent to the ship.

starting in the vicinity of the ship and stretching for a few kilometers behind; occasionally there may be a bright line on one or both edges of the wake [*Lyden et al.,* 1988]. In a wind-roughened sea, the turbulent wake will be smoother than its surroundings, reflecting less energy back to the radar and, thus, appearing dark in the image (see Figure 12.6a). Under low wind conditions, the wake may be slightly rougher than its surroundings and therefore can have a small, but measurable, return and appear faintly brighter than its surroundings. Also when the ship is cruising through a region with plentiful natural slicks, the turbulent wake may break up these slicks, allowing the wind to generate more Bragg waves producing enhanced backscatter (see Figure 12.6b). As the ship passes, the hull movement through the water generates vortices whose surface currents concentrate surfactants at the edges of the turbulent wake. As the wake turbulence dissipates, sometimes the only remaining trace of the wake is these surfactant bands which then appear as dark "railroad tracks" extending in excess of 20 km behind the ship [*Milgram, et al.,* 1993] (see Figure 12.6c).

There are many factors that affect the general probability of detecting ship wakes in SAR imagery including the ship speed, hull shape, wind, sea state, and ship propulsion system [*Peltzer, et al.,* 1987]. The turbulent wake is the most persistent (as well as the most common) wake signature seen in SAR imagery. *Eldhuset* [1996] found that in 200 wake-like features seen in SEASAT L-band imagery, 85% exhibited turbulent wakes of about 2.5 km; and in 180 ERS-1 C-band images, 80% of wakes were turbulent with lengths ranging from 2.7 to 3.3 km. Buoy

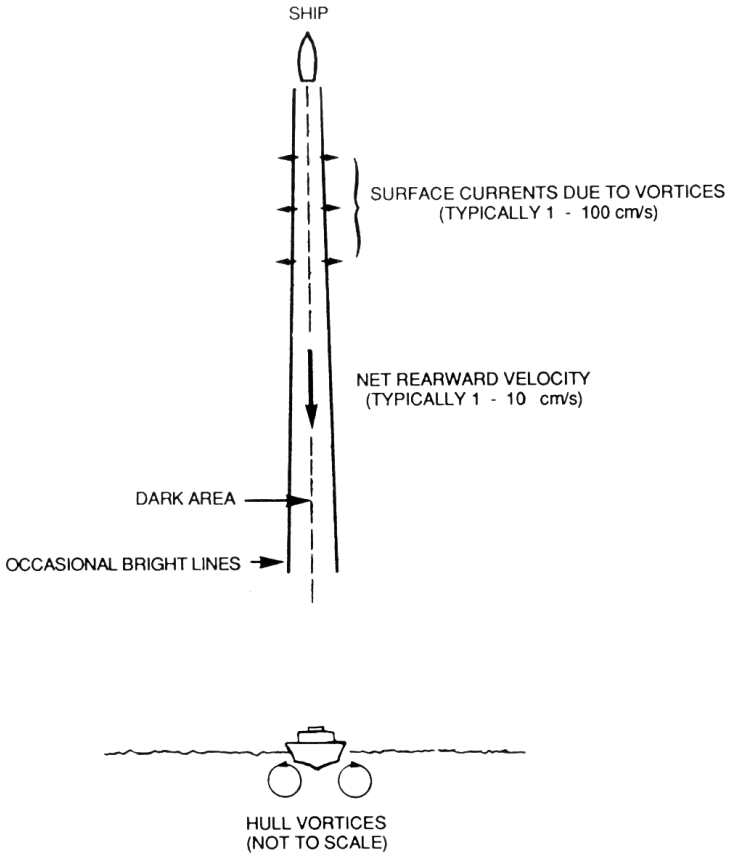

Figure 12.5b (left) Geometry of turbulent wake with associated currents noted. [After *Lyden et al*., 1988].

Figure 12.5c (below) Geometry of Kelvin wake components shown in Figure 12.5a [After *Hennings et al.,* 1999]. Note particularly the location of the cusp waves where the transverse and divergent waves intersect at the Kelvin envelope. These are the largest waves and the ones most often imaged by SAR systems.

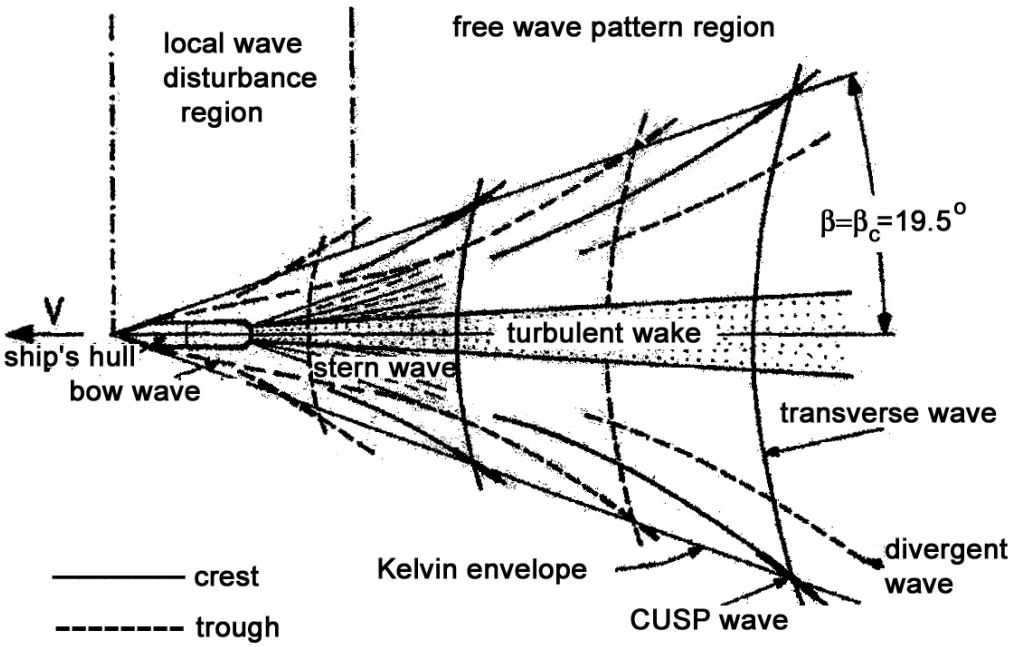

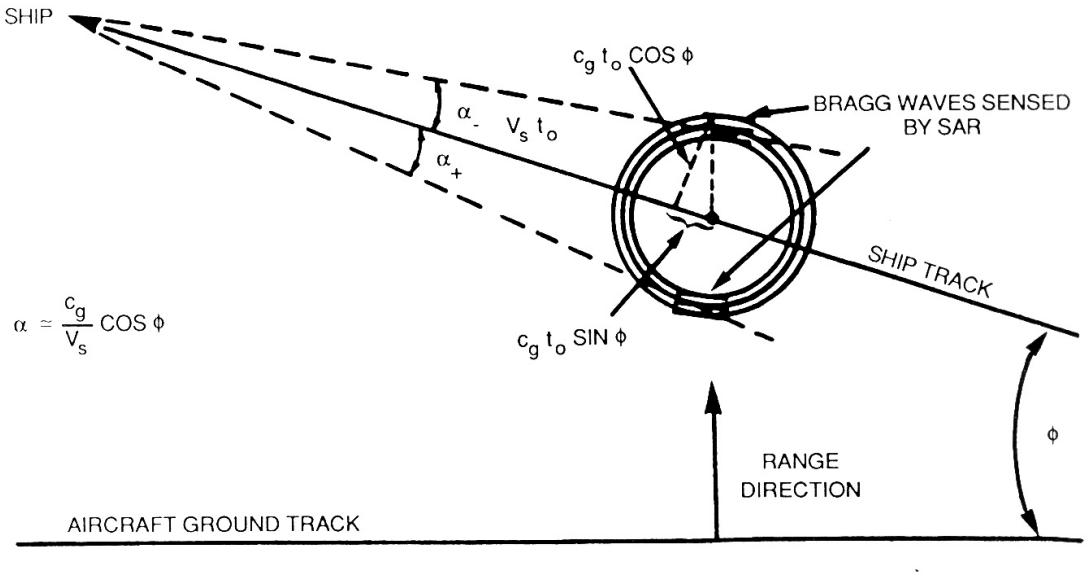

α - SHIP WAKE HALF ANGLE

c_g - GROUP VELOCITY OF BRAGG WAVES

V_s - SHIP VELOCITY

t_o - TIME

ϕ - SHIP HEADING RELATIVE TO AIRCRAFT GROUND TRACK

Figure 12.5d (above) SAR signal return from Bragg waves results in a narrow-V wake seen in SAR imagery under the right environmental conditions [After *Lyden et al.,* 1988].

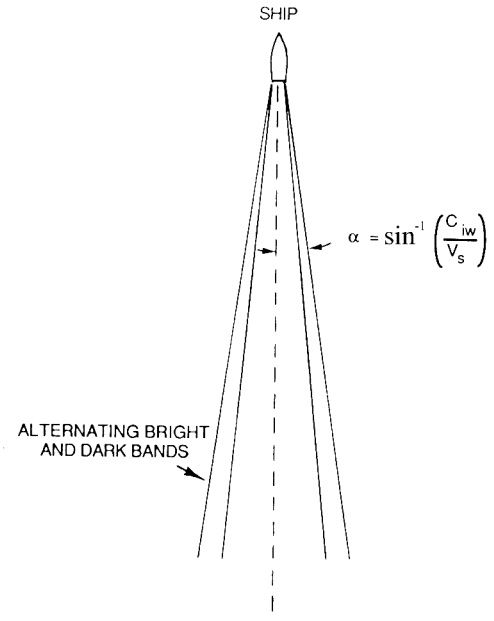

Figure 12.5e (left) Geometry of Internal Wake. Structure of internal waves generated by passage of a ship under conditions of surface water stratification. [After *Lyden et al.,* 1988].

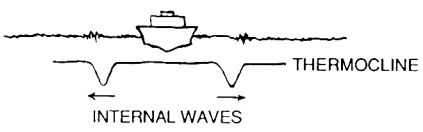

α - SHIP WAKE HALF ANGLE

C_{iw} - INTERNAL WAVE PHASE SPEED

V_s - SHIP VELOCITY

measurements of attenuation of small waves in wakes show that turbulent wakes can exist for more than 10 minutes in oil tanker wakes, even longer (up to an hour) in the greater turbulence within barge wakes or when winds are light. Turbulent wakes are most commonly seen under moderate wind conditions (2.5 to 7.5 m s^{-1}), with longer wakes (up to tens of kilometers) found at the lower end of this wind speed range [*Milgram et al*., 1993]

12.3.2 Kelvin Wakes

The Kelvin wake, first described by Lord Kelvin in 1887 [*Thompson,* 1887], consists of transverse and divergent gravity waves generated by a moving vessel, which interfere to form the cusp waves that are the Kelvin wake structures most often seen in satellite SAR images. As illustrated in Figure 12.5c, transverse waves, propagating approximately in the direction of motion of the ship (i.e., with crests approximately perpendicular to the ship direction), have propagation directions in the range $0^o \leq \phi \leq 35^o16'$, where ϕ is the angle between the ship track and the wave propagation direction (measured from the direction of ship forward movement). The divergent waves propagate outwards at angles approaching directions perpendicular to the ship's direction of motion, in the angular range $35^o16' \leq \phi \leq 90^o$ [*Hennings et al.,* 1999]. These two types of waves interfere to form a V-shaped pattern of cusp waves at regular intervals along the wake at half angles (i.e., one half the interior angle formed by the "V") β of $\pm$ 19.5^o, with the ship approximately at the apex of the "V". This V-shaped pattern is called the Kelvin ship-wave wedge [*Lighthill,* 1978]. The cusp waves are propagating approximately at $\phi = 35^o$ with crests aligned at $\phi = 55^o$ and a wavelength of $4/3\pi V^2 g^{-1}$, where V is the ship speed and g is the acceleration of gravity. It should be noted, however, that these angles and wavelength can change for large slow-moving vessels (when the vessel length l is large compared with V^2/g) or for small speedboats (where l is small compared with $V^2 g^{-1}$). For slow-moving vessels, the dominant wake waves have a wavelength of $2\pi V^2 g^{-1}$ and propagate at small ϕ; for speedboats, the waves are much shorter and propagate at large ϕ, close to $\phi = 90^o$ [*Lighthill,* 1978].

Although not as commonly imaged as the turbulent wake, the Kelvin wake appears in higher resolution SAR imagery, such as 30 m resolution Standard Mode RADARSAT-1 and ERS-1/2 imagery. In ERS-1/2 imagery, the Kelvin wake is visible in about 17% of ship detections [*Melsheimer et al.,* 1999]. One or both of the arms of the Kelvin wake can be imaged as either bright or dark streaks (Figure 12.6d) when wind conditions are moderate (3 to 10 m s^{-1}). The cusp waves usually have the largest amplitude within the Kelvin wake, and are thus more likely to be imaged by a SAR. The cusp waves are generally smeared into a line in the SAR image, at a half angle of approximately $\pm$19.5 degrees. Generally only one of the two Kelvin wake arms is visible in SAR imagery. When the cusp waves are propagating toward or away from the radar look direction, the Kelvin arm is usually bright from an increase in normalized radar cross section; but when the propagation direction is perpendicular to the radar look direction, the Kelvin arm is normally not imaged or can be dark from a reduction in normalized radar cross section [*Hennings et al*., 1999]. The angular difference between the cusp wave propagation directions for the two arms is such that when the cusp waves for one arm are propagating generally in the same direction as the radar look angle, the cusp waves for the other arm are propagating generally perpendicular to the radar look direction. Thus, when one arm is at maximum visibility in the SAR image, the other arm is at minimum visibility or is dark. There are certain ship-heading/radar-look-angle combinations where backscatter from the two arms is relatively equal; however, in general there will be a disparity in visibility.

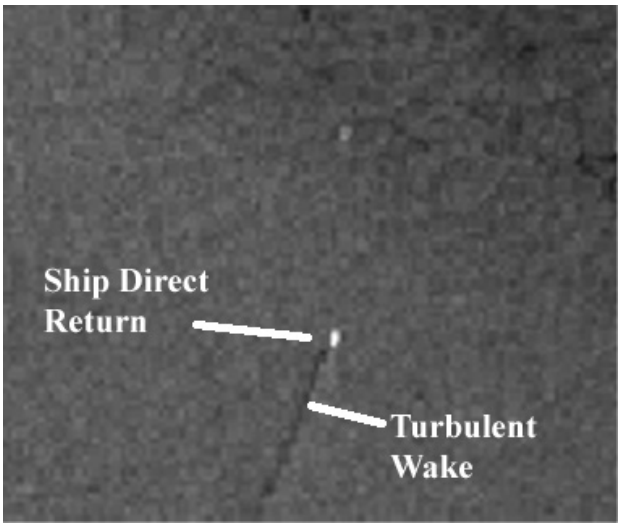

Figure 12.6a (above). RADARSAT-1 (C-band, HH) Standard Mode image acquired 30 July 1998 at 2240 UTC off the coast of New Jersey showing a ship with a dark turbulent wake. The wake is approximately 4 km long in this image. ©CSA 1998

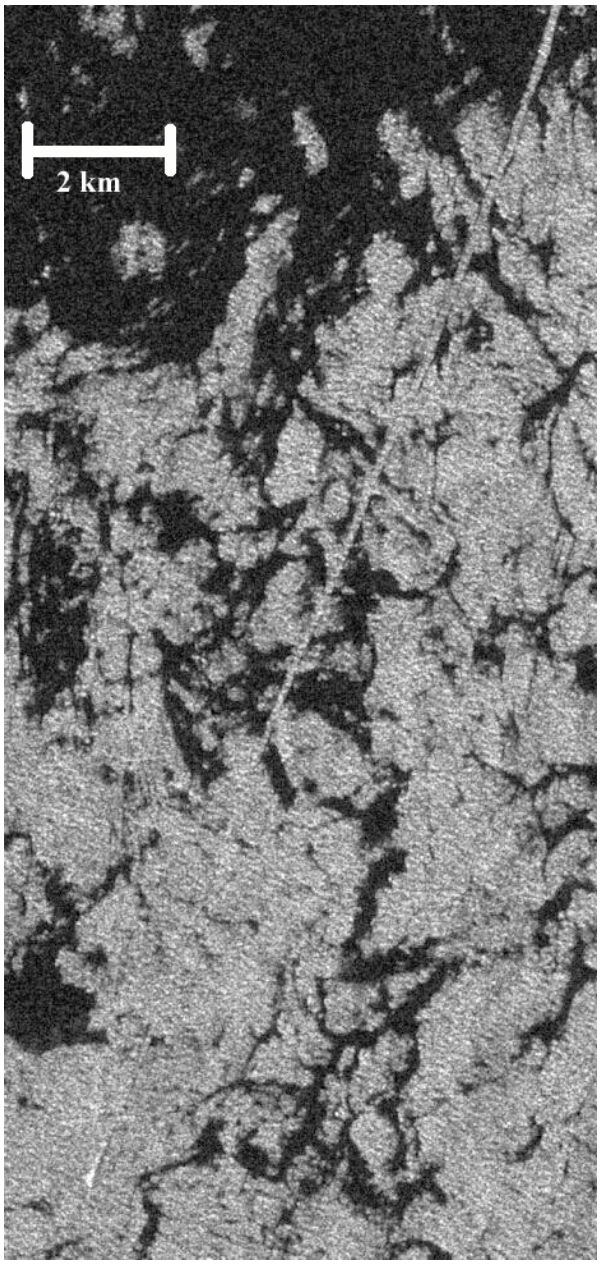

Figure 12.6b (right) ERS-1 (C-band, VV) Standard Mode image acquired 9 April 1996 at 307 UTC showing a bright turbulent wake in the South China Sea (7°54'N; 109°04'E). The turbulent wake from the ship (in the lower left corner of the image) breaks up the natural surface films in this region, allowing the wind to generate Bragg waves which lead to enhanced radar backscatter in the wake. Image is courtesy of Werner Alpers, Institute of Oceanography, Center for Marine and Climate Research, University of Hamburg, Germany. ©ESA 1996

The probability of detecting the Kelvin wake increases with decreasing wind speed, but is almost independent of wind direction. There is very little variation in detection probability with radar frequency, but the probability should increase with decreasing incident angle and should be higher with HH polarization than with VV polarization SAR systems [*Hennings et al.,* 1999]. With current spaceborne systems, however, ERS-1/2 VV polarization images tend to exhibit more wakes than RADARSAT-1 HH polarization images as a result of the greater signal to noise ratios of ERS-1/2 [*Wackerman et al.,* 2001]. But even in ERS-1/2 imagery, wakes are not seen in 37% of all ship targets [*Vachon et al.,* 1997]. V-wakes decay much more rapidly than turbulent wakes and are therefore usually much shorter in SAR imagery.

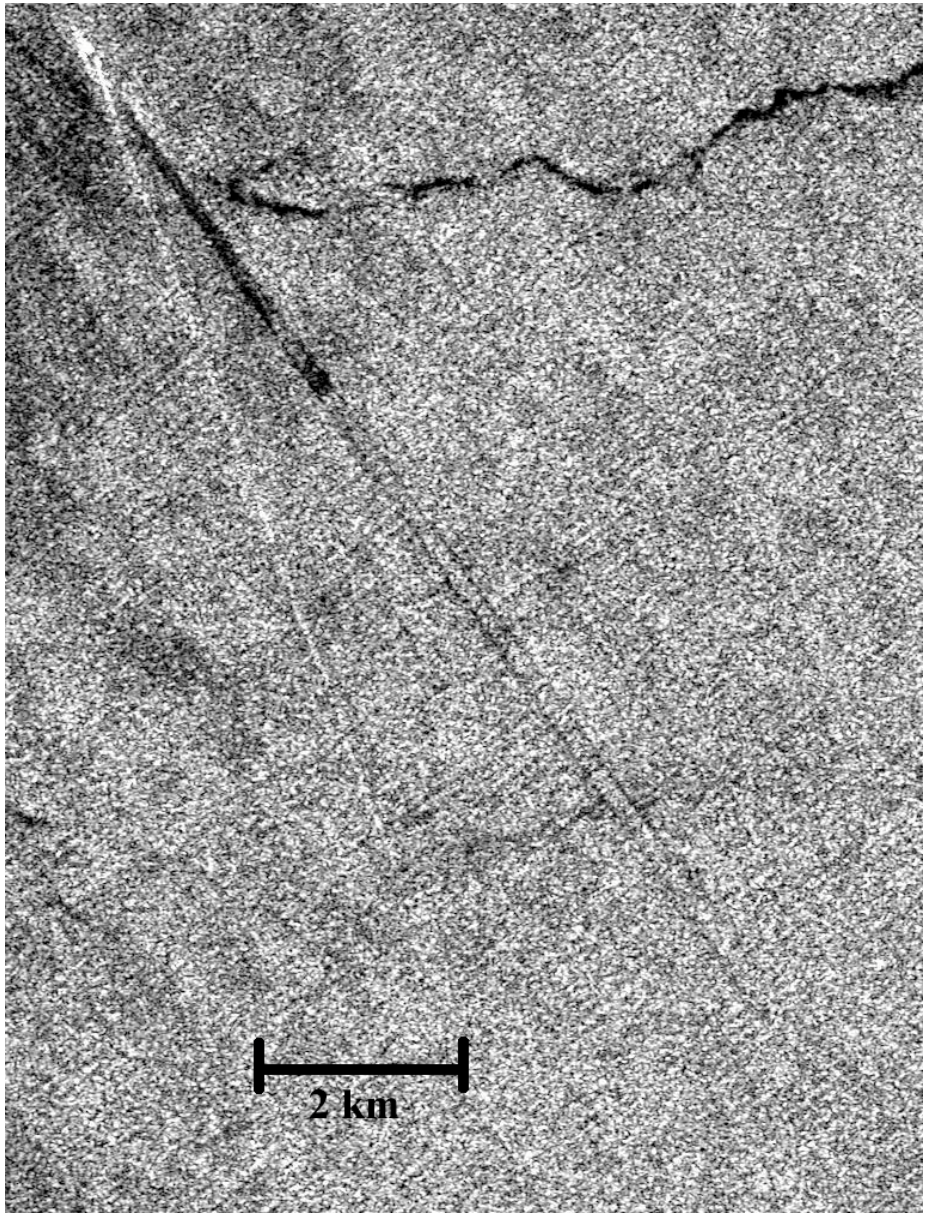

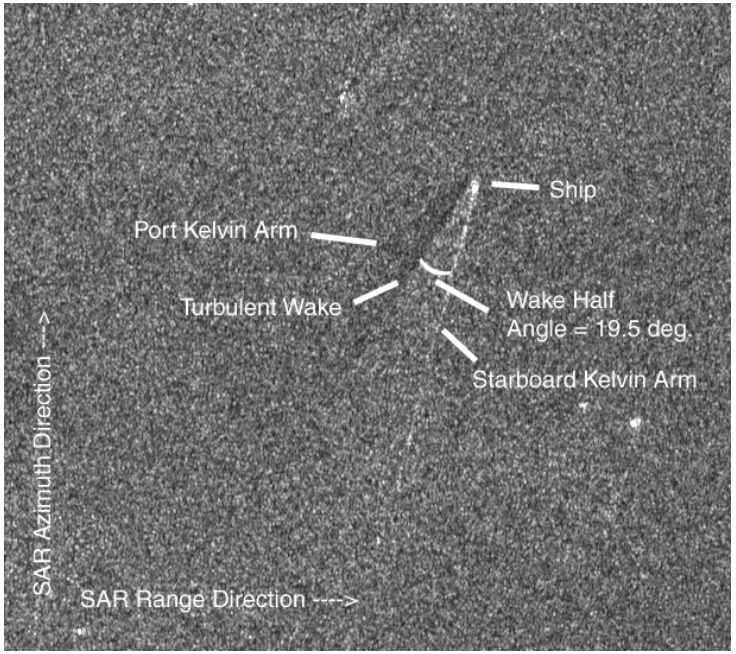

Figure 12.6d (above) RADARSAT-1 (C-band, HH) Standard Mode image acquired 2356 UTC, 15 April 2002 in the Gulf of Mexico near the Louisiana coast. Both arms of the Kelvin wake can be seen, with the port wake visible only faintly. A faint dark turbulent wake is also visible behind the vessel. ©CSA 2002

Figure 12.6c (left) ERS-1 (C-band, VV) Standard Mode image acquired 1600 UTC, 4 May 1996 in the Straits of Malacca (4°36'N; 99°35'E). The long turbulent wake ends in two roughly parallel dark lines reminiscent of railroad tracks. The tracks are likely the result of lingering surface films generated by convergent surface currents at the edges of the turbulent wake. The port-side arm of the Kelvin wake is also imaged (bright line). Image is courtesy of Werner Alpers, Institute of Oceanography, Center for Marine and Climate Research, University of Hamburg, Germany. ©ESA 1996

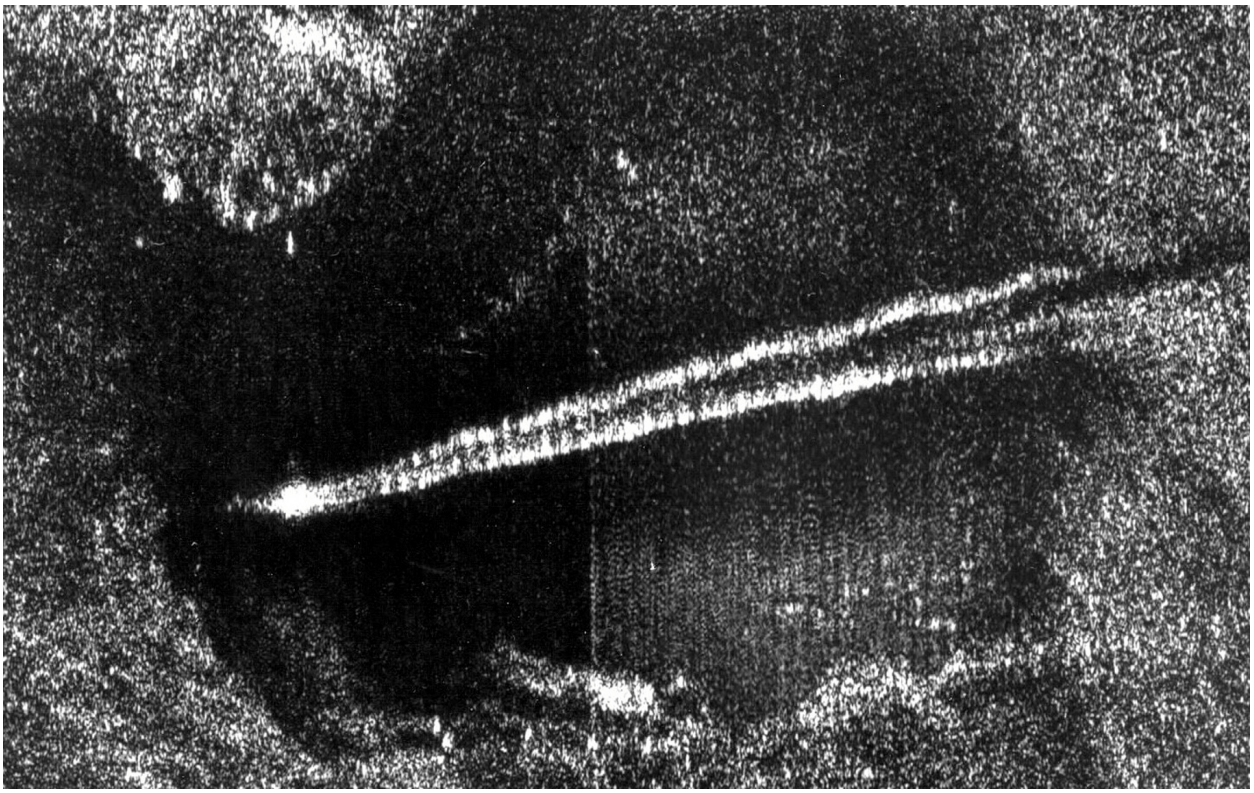

Figure 12.6e. Aircraft SAR (L-band, HH) image of the USS Quapaw in Dabob Bay, Washington, acquired 28 July 1983 during the U.S.-Canada Joint Ocean Wave Investigation Project (JOWIP). The Quapaw was traveling at 8 m s^{-1} and was imaged at an angle of incidence of 27°. The narrow-V wake has a half angle of about 2.5°. Image courtesy of Richard Gasparovic, the Johns Hopkins University Applied Physics Laboratory.

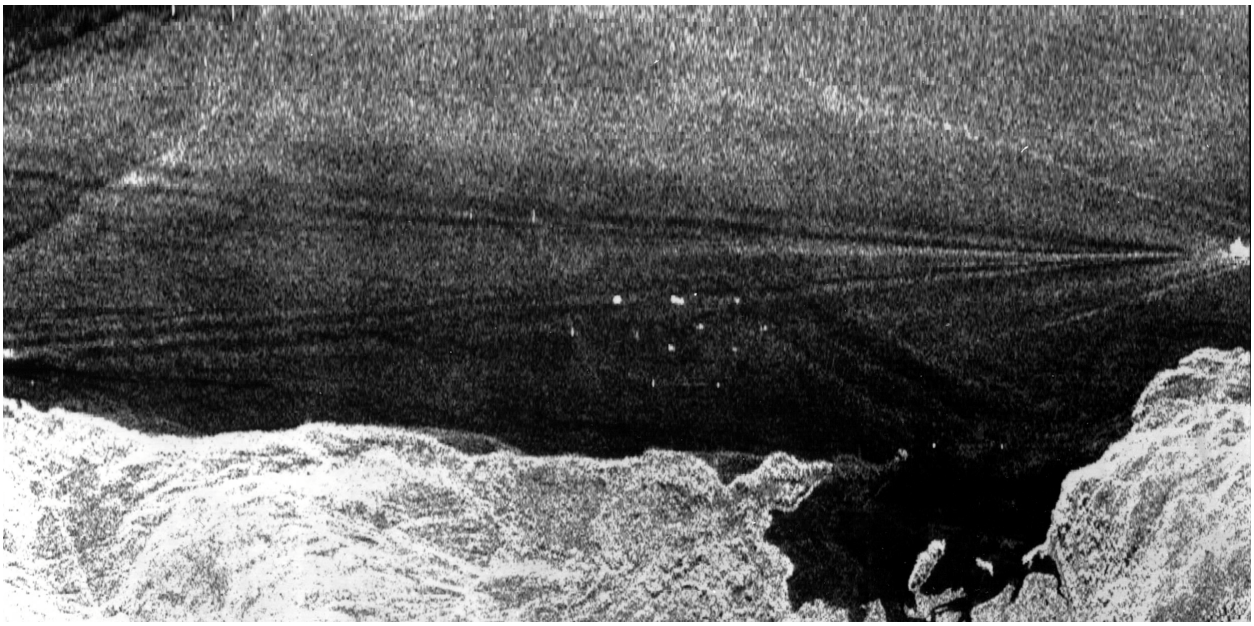

Figure 12.6f. Jet Propulsion Laboratory AIRSAR (L-Band, VV) image acquired on 13 August 1989 showing a ship generated internal wave wake (parallel dark and light bands) in Loch Linnhe, Scotland, a highly stratified fiord. Image courtesy of Richard Gasparovic, The Johns Hopkins University Applied Physics Laboratory.

12.3.3 Narrow-V Wakes

Narrow-V wakes seen sometimes in SAR imagery result from resonant (i.e., enhanced) Bragg scattering of the radar pulses from the short centimeter-scale waves which are generated by the hull moving through the water and which propagate outwards in all directions (Figure 12.5d). Only visible to the eye as very small waves, the characteristic V-shaped pattern of two bright lines is only visible in SAR imagery. Narrow-V wakes have included half angles in the range of 2 to 3 degrees [*Shemdin,* 1990]. The angle is determined by the ratio of the group velocity of the Bragg waves to the ship velocity [*Shemdin,* 1990] and the ship heading relative to the SAR platform's ground track [*Lyden et al.,* 1988]. Figure 12.6e shows a narrow-V wake. Narrow-V wakes are seen in SAR imagery only at low wind speeds (less than 3 m s^{-1}); i.e. in cases where the wind speed is too low to generate sufficient Bragg waves to form a measurable radar backscatter from the surrounding ocean. Narrow-V wakes have been observed in deep and shallow waters regardless of stratification [*Shemdin,* 1990].

12.3.4 Internal Wave Wakes

In cases of stratified surface water with a strong shallow pycnocline (i.e., a region of strong vertical gradient in density), downward displacement of surface water by the ship can generate subsurface (i.e. internal) waves. This results in V-shaped internal wave wakes with half angles, $\beta = \sin^{-1}(c/v)$ where c is the phase speed of the outermost internal wave and v is the ship speed [*Gasparovic, et al.,* 1989]. Ship-generated internal waves move slowly, with a phase speed of about 0.1 to 1.0 m s^{-1}. The half angle thus decreases with increasing ship velocity. The wake consists of internal waves propagating roughly perpendicular to the ship track. As with other types of internal waves (see Oceanic Internal Waves and Solitons, Chapter 7), surface current variations associated with the internal wave interact with small surface Bragg waves resulting in visible wavelike surface roughness changes [*Lyden et al.,* 1988]. See Figure 12.5e.

Internal wave wakes appear as V wakes, but with an alternating dark and bright wave pattern roughly parallel to the ship track. The wake may be a narrow-V or have a half angle even larger than the Kelvin wake. The angle may change along the ship track because the V narrows as the ship speed increases. Because ship-generated internal waves move slowly there are no transverse internal waves generated unless the ship is traveling very slowly, in which case the ship may experience internal wave drag known as the dead water effect [*Watson et al.,* 1992]. Figure 12.6f depicts an internal wave wake.

Internal wave wakes are only observed in regions of shallow water stratification. They are observed under moderate wind conditions (approximately 3 to 10 m s^{-1}). They are more readily apparent in L-band imagery than in X-band or C-band imagery because of the longer persistence of L-band Bragg waves [*Lyden et al.,* 1988]. Internal wave wakes are more distinct if the SAR sensor is viewing perpendicular to the ship track. Internal waves (and indeed ocean waves and wakes in general) are much more apparent in higher-resolution SAR imagery (e.g., Standard Mode) than in ScanSAR imagery.

12.4 Slicks

Although the topic of slicks is addressed in detail in Chapter 11, ship-related slicks are mentioned in this chapter to complete the discussion of phenomena related to ship detection.

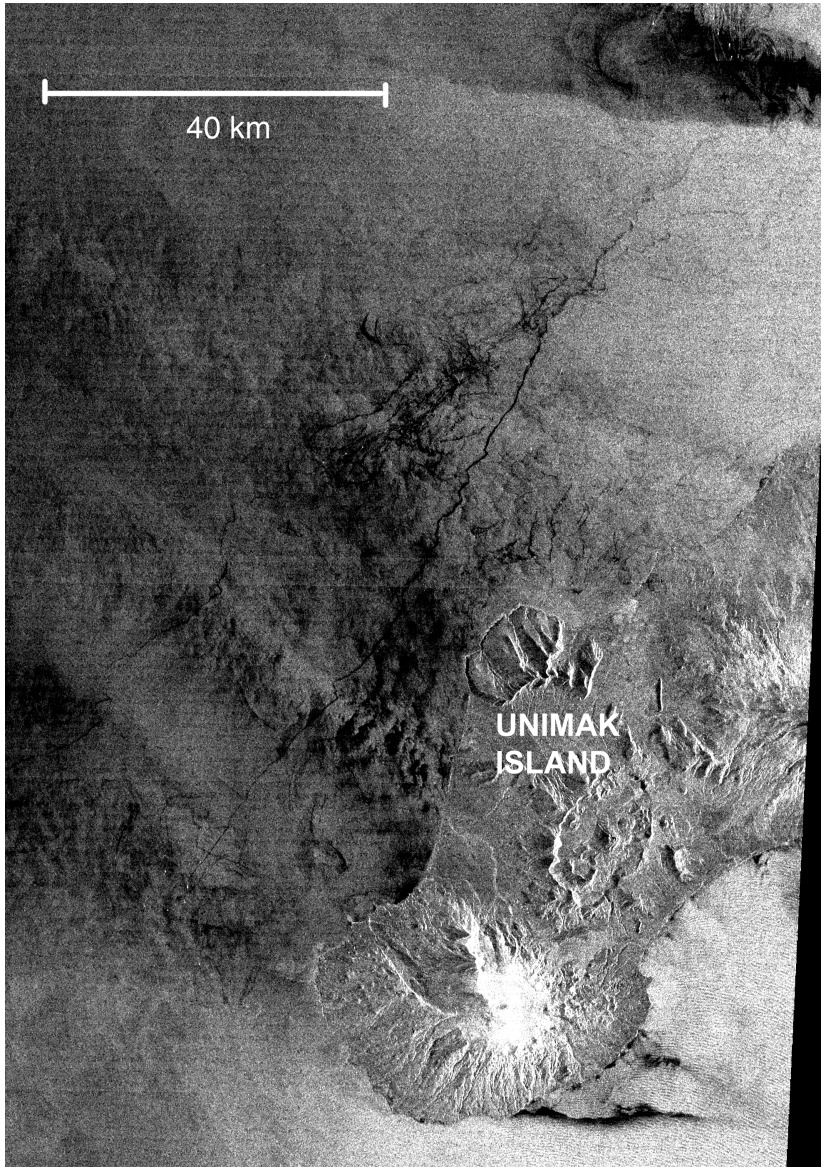

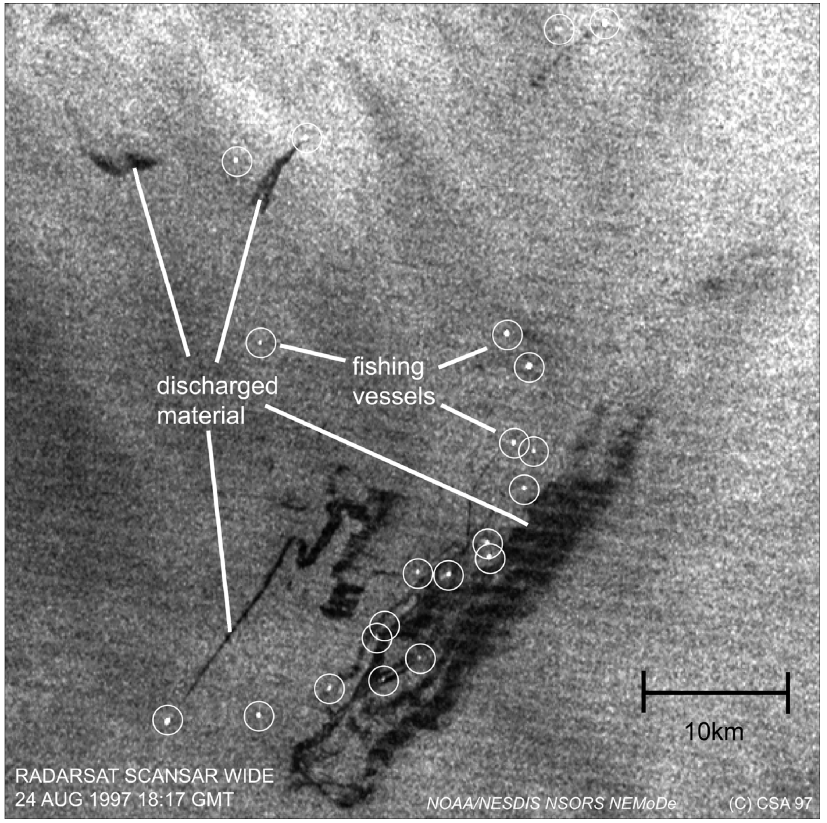

Figure 12.7b (above). RADARSAT-1 (C-band, HH) ScanSAR Wide B image from the Bering Sea (acquired 24 August 1997 at 1817 UTC) showing a fleet of vessels with at least some of the vessels fishing in a grid-like pattern, releasing fish oils during catch processing as they continue to fish. The resulting persistent, dark, turbulent wake reveals the pattern of fishing. ©CSA 1997

Figure 12.7a (left) RADARSAT-1 (C-band, HH) ScanSAR Wide B image of Walleye Pollack fishery in the Bering Sea, acquired 20 February 1998 at 1729 UTC. The long slick behind one of the vessels underway extends for over 100 km. ©CSA 1998

Figure 12.7c (above). RADARSAT-1 (C-band, HH) ScanSAR Wide B image acquired on 12 September 2000 at 1825 UTC in the vicinity of the U.S./Russian maritime border near Cape Navarin in the Bering Sea. Many ships are evident, but almost none are associated with the dark slick features, which presumably were created during past fish processing or fishing activity and persist even after the vessels have moved on to other areas. ©CSA 2000.

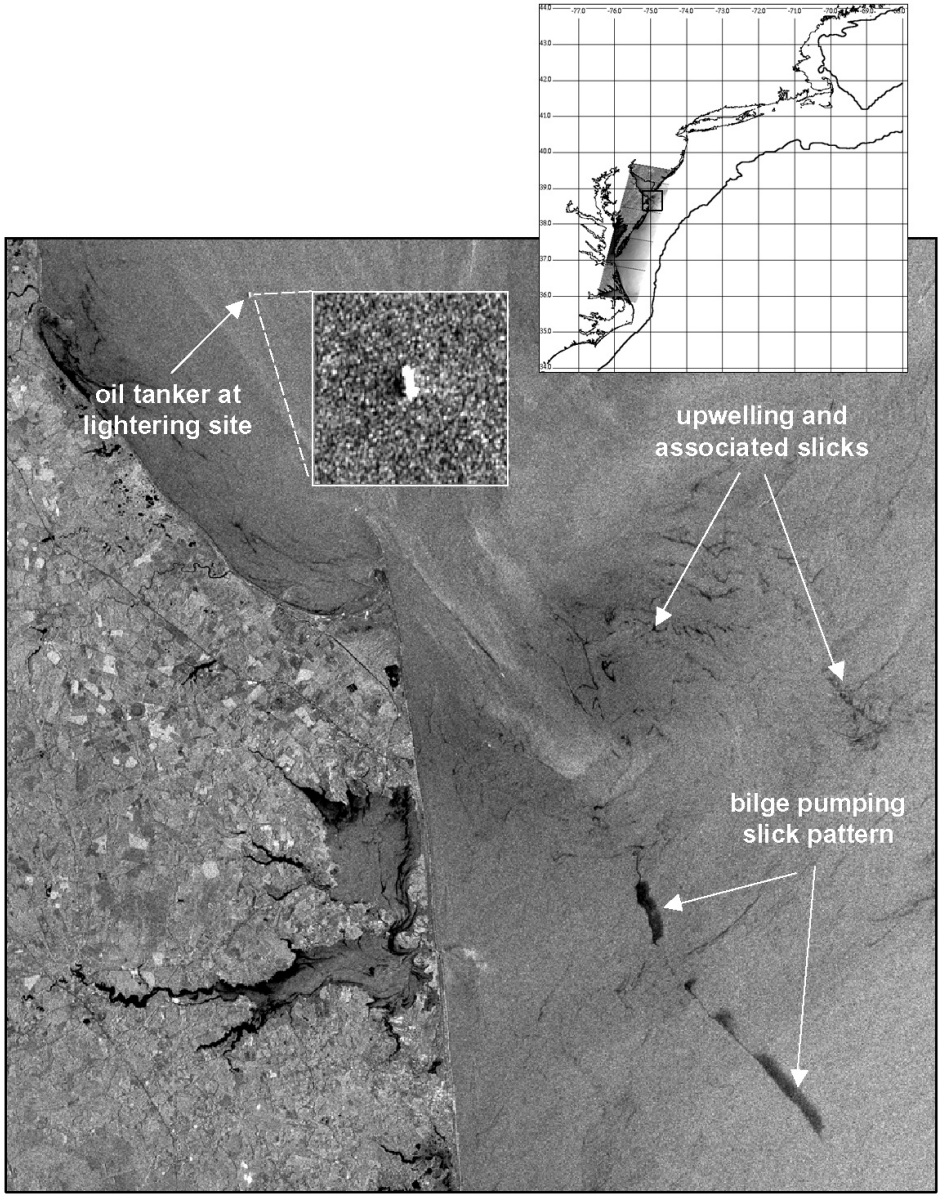

Figure 12.7d (right) RADARSAT-1 (C-band, HH) Standard Mode SAR image acquired 12 August 1998 at 1115 UTC showing a bilge-pumping slick pattern generated by a ship on its way into Delaware Bay [*Clemente-Colón*, 2001] ©CSA 1998.

12.4.1 Physical Process

In addition to natural surfactants brought to the surface in a turbulent wake, other processes can lay down long-lasting surfactant slicks behind a ship. Fish-oil release as a result of catch boarding and processing activities, or inadvertent (or deliberate) release of petroleum products (e.g., during normal engine operation or as a result of bilge pumping) can generate surfactant slicks. These slicks dampen small-scale surface waves and thus manifest as a dark wake behind a vessel, sometimes stretching for a hundred kilometers [*Clemente-Colón,* 1998], and thus forming some of the longest ship-related ocean disturbances.

12.4.2 SAR Imaging Characteristics and Limitations

The presence of slicks in the wake of a ship will result in enhanced and prolonged backscatter suppression in the wake, such as is shown in Figure 12.7a. If a vessel is actively fishing or processing catch with concomitant release of fish oils, the pattern of movement of the fishing fleet or the fishing pattern of individual vessels can be deduced [*Montgomery,* 2000; Figure 12.7b]. Under some environmental conditions, these fishing slicks can persist even after the vessels have moved to other fishing grounds [Figure 12.7c; *Clemente-Colón et al.,* 1998]. Finally, bilge pumping often leads to a tell-tale broadening of the turbulent wake as a ship approaches harbor (Figure 12.7d). For these ship-related slicks to be visible, there must be substantial release of surfactants. There must also be moderate wind—enough to form small waves that are damped by the surfactant, but not enough to mix the surfactant down out of the surface skin.

12.5 Other Ship-Related Phenomena

In addition to cases where surfactant slicks indicate recent vessel activity even when no vessel remains, there are other cases where only V-wakes are seen, but one is led to deduce that the vessel is still in the area viewed. The ship may be too small or made of low radar-reflective material and consequently cannot provide a hard target return under the existing sea conditions. Submarines traveling near the surface may also leave wakes [*Liu,* 1996]. See Figure 12.8.

Another interesting SAR image phenomenon related to ship detection is the displacement in the SAR image of a rapidly moving ship under certain viewing angles. A moving ship with a substantial velocity component in the radar range direction (i.e., a ship traveling relatively perpendicular to the direction of motion of the SAR satellite) will be displaced (in the SAR image) off its turbulent wake or off the apex of its V-wake by a distance proportional to this velocity component. This is a SAR imaging artifact resulting from placing the ship in a different image azimuth location (i.e., in the image dimension parallel to the satellite motion) than the ocean pixels surrounding the ship, as a result of the extra Doppler shift from the ship's motion relative to the sea surface. A SAR processor maps the azimuth location of an object based on its Doppler history. If a ship is moving away from the SAR platform, its image will be displaced in the negative azimuth direction (opposite to the SAR platform direction of motion); motion toward the SAR platform will result in positive azimuth displacement (See Figure 12.9). This phenomenon is similar to the "train off the track" artifact seen when imaging moving trains with SAR.

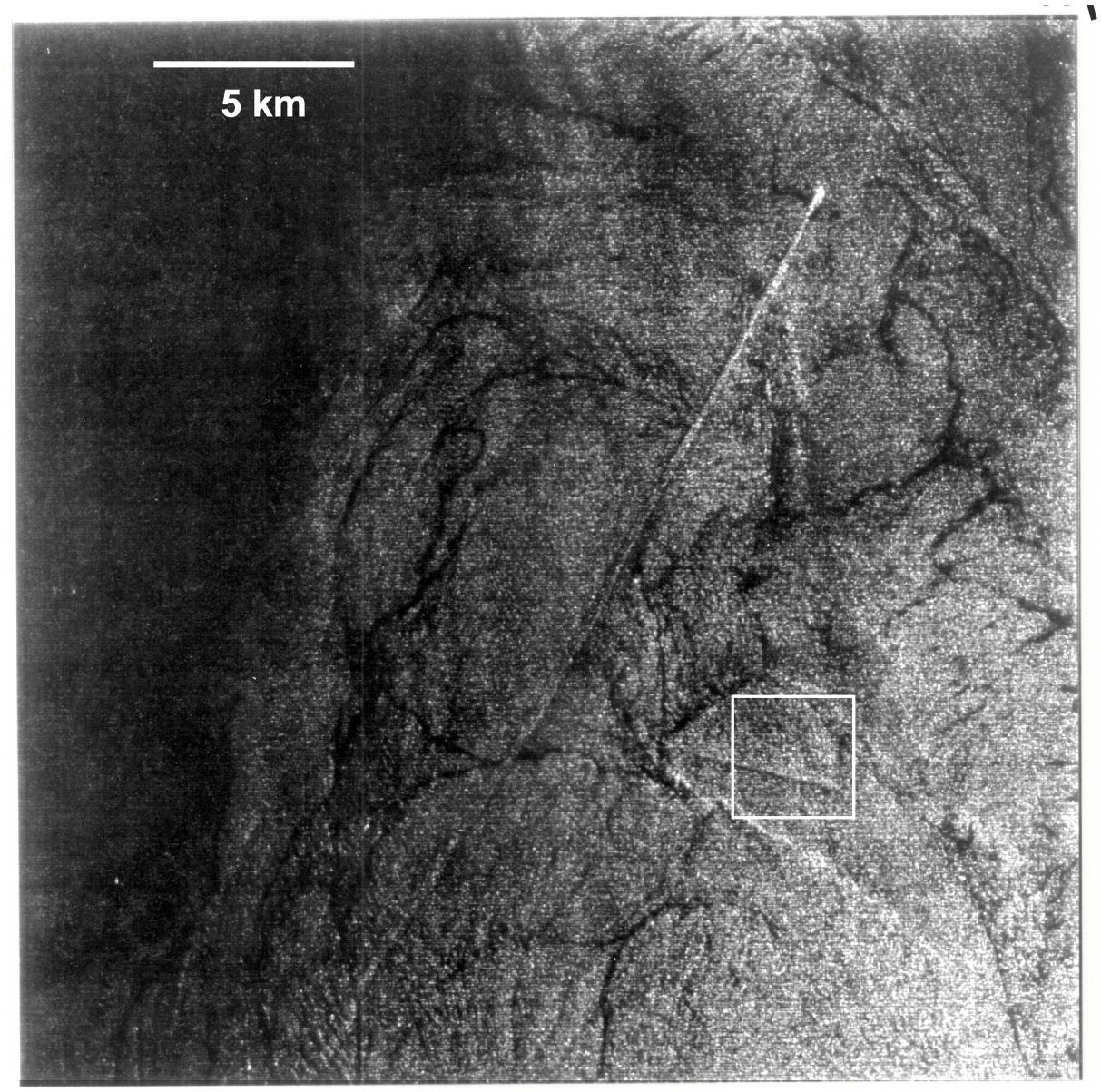

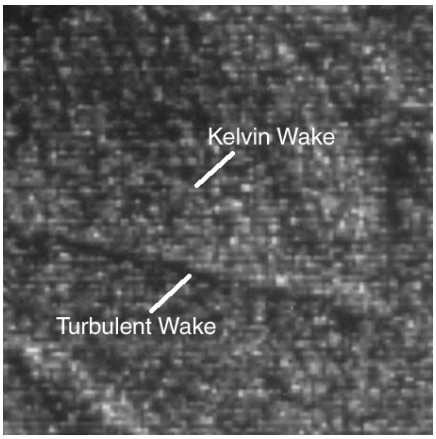

Figure 12.8a (above). This is a 25 km x 25 km sector of and ERS-1 SAR image acquired 31 May 1995, north of Taiwan in the East China Sea at 25.62°N and 121.15°E [*Liu,* 1996]. The water depth is about 100 meters. A ship bright turbulent wake can be seen stretching across the image from lower left to upper right with a ship direct return at the end of the wake in the upper right corner. Inside the square is another turbulent wake and, faintly, one arm of the Kelvin wake for a vessel traveling to the right (east); however, in this case, despite the presence of a wake, there is no bright direct return from a ship. Figure 12.8b (left) is an annotated enlargement of the portion of Figure 12.8a enclosed in the white square. The wake structures could have been formed by a small ship, a ship made of low radar-reflective material such as wood or fiberglass, or perhaps a submarine traveling close to the surface [*Liu*, 1996]. Original image ©ESA 1995.

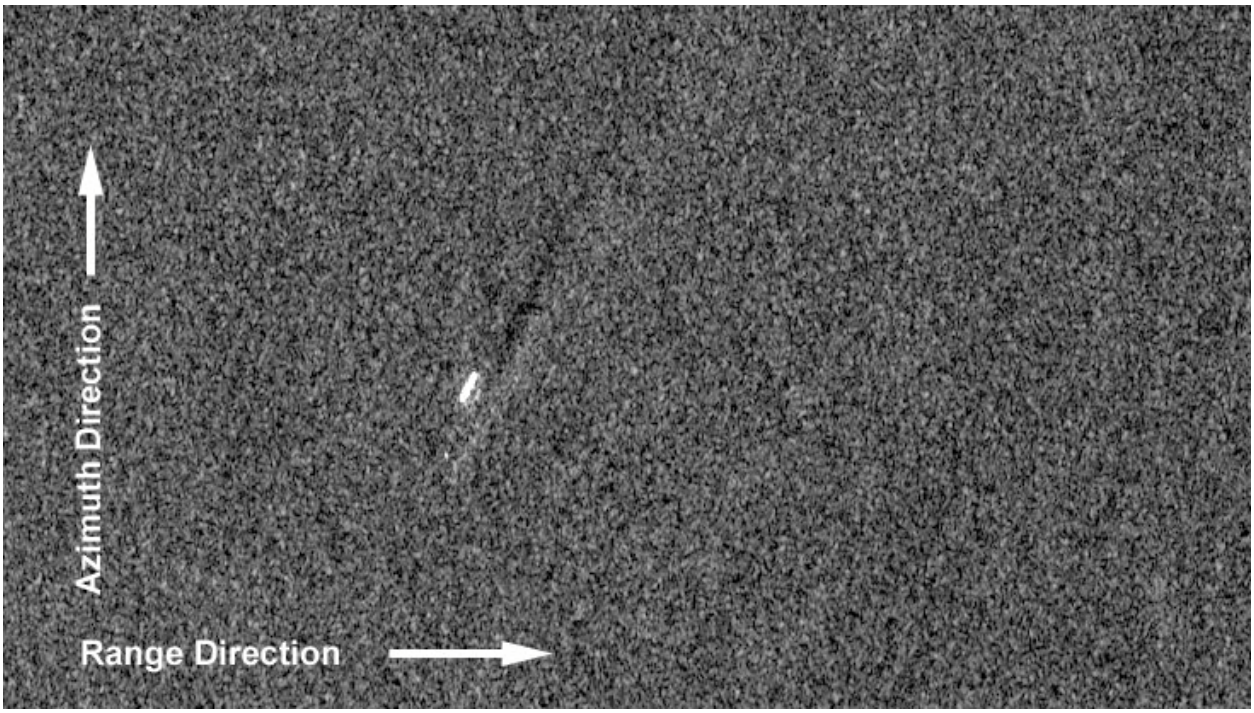

Figure 12.9 RADARSAT-1 (C-band, HH) Standard Mode image of a ship displaced from its wake. The image was acquired on 5 November 1997 at 1111 UTC. The ship is located off the East Coast of the U.S. near Chesapeake Bay. ©CSA 1997

12.6 Ship Detection Applications Demonstration

Competition for dwindling fishery resources, increased emphasis on protection of endangered species, and a desire to improve safety of life and property under dangerous environmental conditions have all led to an increased need for adequate management and enforcement of fisheries. Traditionally, fisheries management has been accomplished through use of onboard observers or aircraft surveillance. However, both are expensive and the latter is hampered by weather, darkness, and the large regions that must be surveyed for open ocean fisheries. Detection of vessel positions using SAR imagery is a tool useful in aiding management and enforcement of fisheries. Techniques have been developed to automatically detect vessels in SAR images and provide these vessel positions to agencies responsible for fisheries resource management and protection. These techniques are being used routinely, if not operationally, at a number of facilities around the world. For example, routine ship detection and oil spill products are generated by Kongsberg Satellite Services (formerly the Tromsø Satellite Station) in Norway [*Vachon and Olsen*, 2000], at the European Space Agency European Space Research Institute in Fucino, Italy, [*Cusano et al.,* 2000], and by the Canadian Department of Fisheries and Oceanography Canada within the Ocean Monitoring Workstation [*Henschel et al.,* 1997; *Vachon et al.,* 2000]. In the U.S., NOAA is conducting an applications demonstration in Alaska [*Pichel and Clemente-Colón,* 2000], where vessel positions are generated each day from images of the Bering Sea and Gulf of Alaska received in near real-time from the Alaska Satellite Facility (ASF) at the University of Alaska Fairbanks. These vessel positions are being used to monitor the U.S./Russia maritime border, to monitor coastal and open ocean fisheries activities, and to monitor environmental hazards such as ice and severe storms, which impact the safety of the fishing fleet.

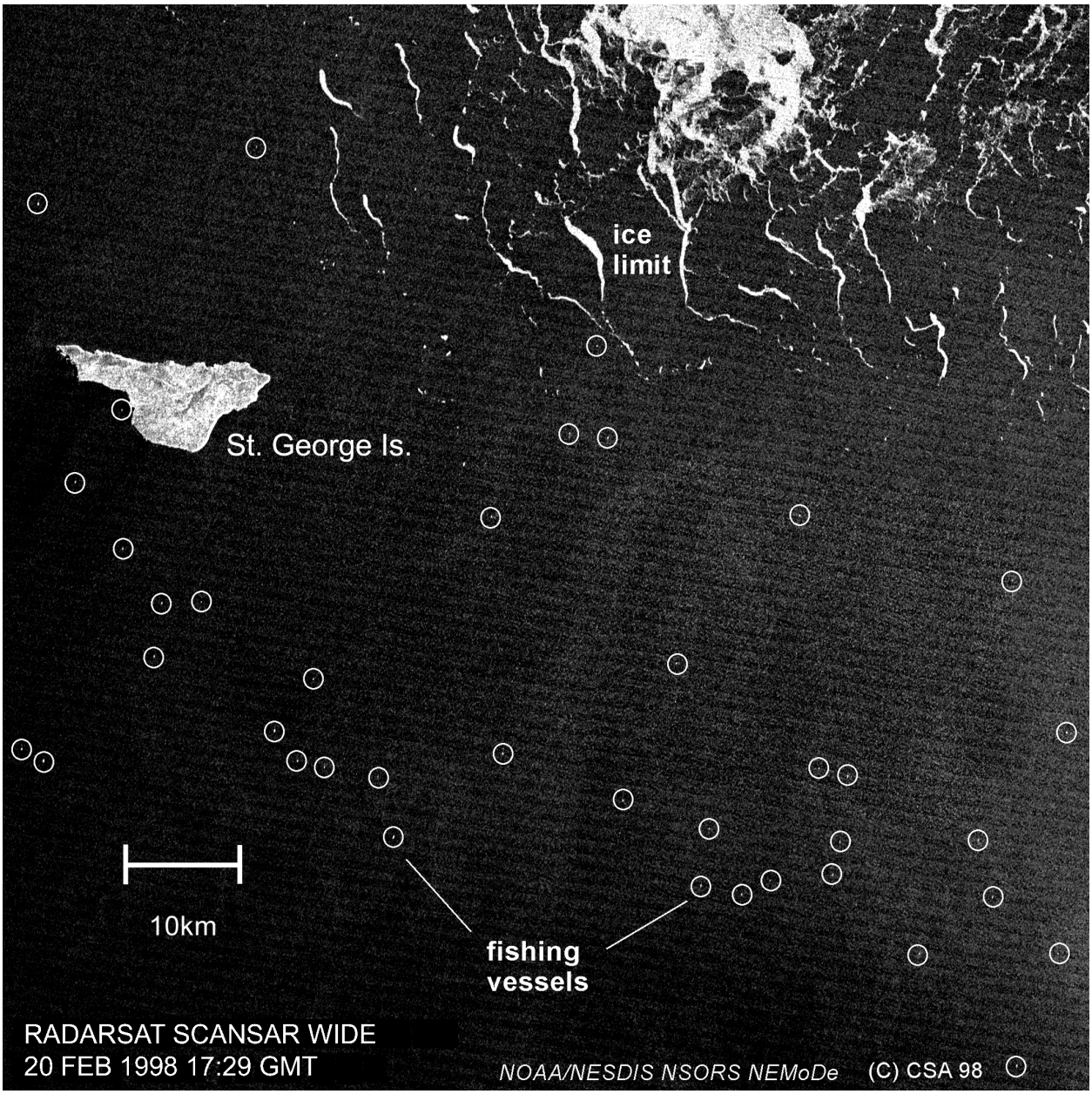

Figure 12.10. A portion of a RADARSAT-1 (C-band, HH) ScanSAR Wide B image acquired 20 February 1998 at 1729 UTC showing snow crab fishing vessels near the ice edge in the region of St. George Island in the Bering Sea. ©CSA 1998.

During this NOAA Alaska SAR Demonstration (AKDEMO), the utility of the vessel positions has been assessed for a number of fisheries, including Alaskan crab fisheries. There are two open-ocean crab seasons in Alaska, the snow crab season held usually in January and February north of the Aleutian Islands in the Bering Sea and the red crab season in October in Bristol Bay, north of the Alaska Peninsula. Both fisheries employ similar steel-hulled vessels typically ranging in length from 15 to 61 meters, with the majority of vessels in the range 24 to 41 meters.

The snow crab (Chinoecetes opilio) fishery in Alaska is among the most dangerous fisheries in the world. During the snow crab season in 1999, 11 seamen died and another 14

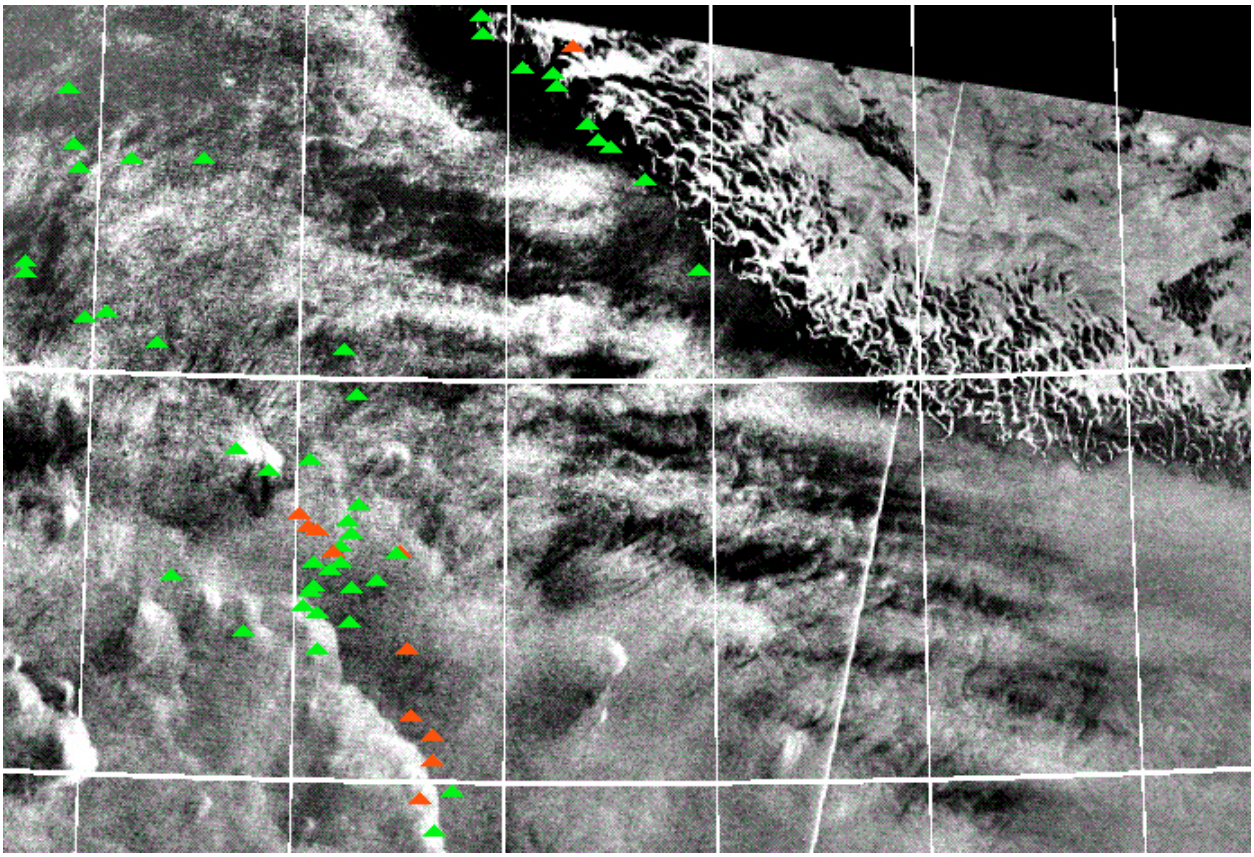

Figure 12.11 Ships detected in a RADARSAT-1 (C-band, HH) ScanSAR Wide B scene acquired on 4 April 2000. Vessels are in the Alaskan snow crab fishery. Triangles indicate automated detections of open ocean vessels (or ship-sized ice pieces). Green detections are strong, red are weak. Detections in the upper middle of the image are probably ice pieces located along the edge of the ice pack. © CSA 2000.

were seriously injured [*Gary Hufford,* 1999, personal communication]. This fishery usually occurs in the vicinity of the southern limit of ice in the Bering Sea during a time of year when severe weather is likely. Intense cold, superstructure icing, and dangerous wave and wind conditions from rapidly developing polar mesoscale cyclones combine to make this fishery particularly hazardous. The fishery is regulated by both the Alaska Department of Fish and Game and the NOAA National Marine Fisheries Service. Weather forecasts are provided to the fleet by the National Weather Service Forecast Office in Anchorage. Figure 12.10 shows the distribution of the snow crab fleet in February 1998 as imaged by a RADARSAT-1 ScanSAR Wide image (100 m resolution). Features of interest are the large number of vessels and the proximity of many of the vessels to the ice edge (threatening life and property should there be sudden movement of ice). A pre- operational test of the AKDEMO ship-detection products in support of this fishery was conducted in April 2000. The winter of 2000 was an especially heavy ice year, so much so that the snow crab season was delayed until April. The season was shortened to only one week beginning April 1 and ending April 8. In this year, the fleet was imaged with SAR two days out of the seven. Figure 12.11 shows a SAR image taken on April 1 with automatically detected ships superimposed. Ship position information was sent to the Alaska Department of Fish and Game and entered into a geographic information system (GIS) for plotting on the maps shown in Figures 12.12a and 12.12b. Total vessel counts and observer reports indicate that the SAR vessel detection algorithm observed a bit less than half of the total

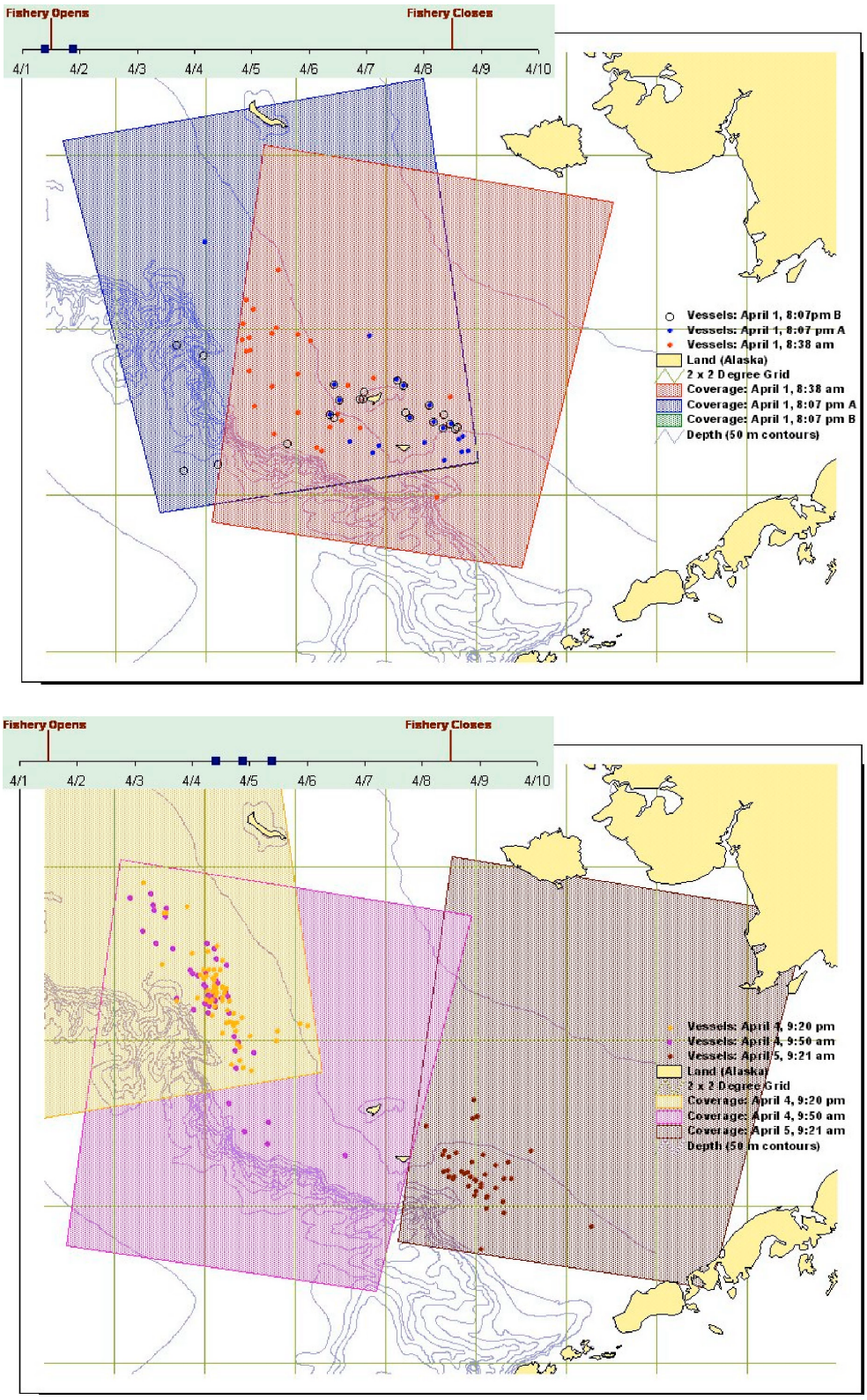

Figure 12.12. These GIS maps of the position of the snow crab fleet on 1 April 2000 (Top) and 4 April 2000 (Bottom) were compiled using automated ship reports from a number of RADARSAT-1 (C-band, HH) ScanSAR Wide B images, including from the image shown in Figure 12.11. Figures courtesy of Fritz Funk, Alaska Department of Fish and Game.

number of vessels in the Alaskan crab fleet [*Friedman et al.,* 2000]. The SAR ship positions indicate that between April 1 and 4, the fleet split into two areas of fishing concentration. This information on overall fleet movement may be as valuable as knowing exactly where all the vessels are. Knowing where the fleet is located allows one to determine whether observer reports (on 10% of the vessels) are representative of the entire fleet.

Vessel Monitoring Systems (VMS) are increasingly required to be used on registered fishing vessels worldwide [*Montgomery,* 2000; *Kourti et al.,* 2001]. These systems automatically report vessel position to enforcement agencies when queried or on a regular schedule. The combination of VMS reporting of registered vessels and detection with SAR of unregistered vessels can be a valuable combination for fisheries management and enforcement.

12.7 Summary

In this chapter we have examined the many aspects of SAR ship signatures and their detection. The most common ship signature is the direct return of the SAR signal from the ship superstructure, appearing in a SAR image as a pixel or group of pixels significantly brighter than the surrounding ocean. Wake signatures are the next most common signature. They include the turbulent wake directly behind the ship, the Kelvin wake with an interior half angle of 19.5^{o}, narrow-V wakes under low wind conditions, and internal wave wakes under conditions of stratified surface water. Finally, the presence of patterns of surface slicks such as long dark turbulent wakes and grid patterns indicative of fishing activity are useful in identifying ships releasing engine or fish oils. Automated techniques have been developed for detecting the direct return from ships. These often employ constant false alarm rate algorithms to handle variations in ship/ocean contrast due to changing wind conditions and radar angle of incidence. Limitations to ship detection success include the physical characteristics of the ship such as size and composition, environmental conditions such as wind and presence of ice, radar characteristics such as angle of incidence and polarization, and SAR image quality and resolution. Despite these limitations, satellite SAR systems can provide valuable information on the location and distribution of fishing and marine transportation vessels, information of use to coastal and fishery managers, law enforcement agencies, and environmental scientists.

12.8 References

Clemente-Colón, P., 2001: Coastal oceanography applications of spaceborne Synthetic Aperture Radar (SAR) in the Middle Atlantic Bight (MAB). Ph.D. dissertation, University of Delaware, Newark, 233 pp.

——, D. Montgomery, W. Pichel, and K. Friedman, 1998: The use of synthetic aperture radar observations as indicators of fishing activity in the Bering Sea. *J. Adv. Mar. Sci. Technol. Soc.,* **4**, 249–258.

Cusano, M., J. Lichtenegger, P. Lombardo, A. Petrocchi, and D. Zanovello, 2000: A real time operational scheme for Ship traffic monitoring using quick look ERS SAR images. *Proc. 2000 Int. Geosciences and Remote Sensing Symp.,* Honolulu, HI, IEEE, 2918-2920.

Eldhuset, K., 1996: An automated ship and ship wake detection system for spaceborne SAR images in coastal regions. *IEEE Trans. Geosci. Remote Sens.,* **34**, 553–560.

Friedman, K., C. Wackerman, F. Funk, K. Rowell, W. Pichel, P. Clemente-Colón, and X. Li, 2000: Validation of an automated vessel detection algorithm using SAR data and known vessel fleet distributions. *Proc. 2000 Int. Geosciences and Remote Sensing Symp.,* Honolulu, HI, IEEE, 2071–2073.

Gasparovic, R., D. Thompson, and J. Apel, 1989: Synthetic aperture radar imaging of ship-generated internal waves. *Johns Hopkins APL Tech. Dig.*, **10**, 326–331.

Hennings, I., R. Romeiser, W. Alpers, and A. Viola, 1999: Radar imaging of Kelvin arms of ship wakes. *Int. J. Remote Sens.*, **20**, 2519–2543.

Henschel, M., R. Olsen, P. Hoyt, and P. Vachon, 1997: The ocean monitoring workstation: Experience gained with RADARSAT. *Proceedings Geomatics in the ERA of RADARSAT (GER'97)*, CD-ROM Proceedings, Ottawa, Canada. Canadian Centre for Remote Sensing, Natural Resources Canada, 12 pp.

Kourti, N., I. Shepherd, D. Brock, S. Moesel, P. Griffith, and D. Martin, 2000: Ship detection for fisheries monitioring. *Backscatter,* **11**, 16–20.

——, ——, G. Schjwartz, and P. Pavlakis, 2001: Integrating spaceborne SAR imagery into operational systems for fisheries monitoring. *Can. J. Remote Sens.,* **27**, 291–305.

Lighthill, J., 1978: *Waves in Fluids.* Cambridge University Press, 504 pp.

Liu, A., 1996: Mystery ship detected in SAR image. *EOS, Trans. Amer. Geophys. Union*, **77**, 17–18.

Lyden, J., R. Hammond, D. Lyzenga, and R. Shuchman, 1988: Synthetic aperture radar imaging of surface ship wakes. *J. Geophys. Res.,* **93** (C10), 12 293–12 303.

Melsheimer,C., H. Lim, and C. Shen, 1999: Observation and analysis of ship wakes in ERS-SAR and Spot images, *Proceedings 20th Asian Conference on Remote Sensing,* Hong Kong, China, Asian Association of Remote Sensing, 3 pp.

Milgram, J. H., R. D. Peltzer, and O. M. Griffin, 1993: Suppression of short sea waves in ship wakes: Measurements and observations. *J. Geophys. Res.*, **98** (C4), 7103–7114.

Montgomery, D., 2000: International fisheries enforcement management using wide swath SAR. *Johns Hopkins APL Tech. Dig.,* **21**, 141–147.

Peltzer, R. D., W. D. Garrett, and P. M. Smith, 1987: A remote sensing study of a surface ship wake. *Int. J. Remote Sens.*, **8**, 689–704.

——, O. M. Griffin, W. R. Barger, and J. A. C. Kaiser, 1992: High-resolution measurement of surface-active film redistribution in ship wakes. *J. Geophys. Res.*, **97** (C4), 5231–5252.

Pichel, W. and P. Clemente-Colón, 2000: NOAA CoastWatch SAR applications and demonstration. *Johns Hopkins APL Tech. Dig.,* **21**, 49–57.

Shemdin, O., 1990: Synthetic aperture radar imaging of ship wakes in the Gulf of Alaska. *J. Geophys. Res*., **95** (C9), 16 319–16 338.

Thompson, W., 1887: On the waves produced by a single impulse of water of any depth or in a dispersive medium. *Proc. Roy. Soc. London,* **42A**, 80–85.

Touzi, R., F. Charbonneau, R. Hawkins, K. Murnaghan, and X. Kavoun, 2001: Ship-sea contract optimization when using polarimetric SARS. *Proc. 2001 Int. Geosciences and Remote Sensing Symp.,* Sydney, Australia, IEEE, 426-428.

Vachon, P., and R. Olsen, 1998: RADARSAT: Which mode should I use? *Backscatter,* **9(4)**, 15–20.

——, and ——, 2000: Ship detection with satellite-based sensors: A summary of workshop presentations. *Backscatter,* **11(4)**, 23–26.

——, J. Campbell, C. Bjerkelund, F. Dobson, and M. Rey, 1997: Ship detection by the RADARSAT SAR: Validation of detection model predictions. *Can. J. Remote Sens.,* **23**, 48–59.

——, S. J. Thomas, J. Cranton, H. R. Edel, and M. D. Henschel, 2000: Validation of ship detection by the RADARSAT synthetic aperture radar and the ocean monitoring workstation. *Can. J. Remote Sens.,* **26**, 200–212.

Wahl, T., K. Eldhuset, and Å Skøelv, 1993: Ship traffic monitoring using the ERS-1 SAR. *Proc. First ERS-1 Symp.—Space at the Service of our Environment,* Cannes, France, ESA, Publ. SP-359, 823–828.

Wackerman, C., K. Friedman, W. Pichel, P. Clemente-Colón, and X. Li, 2001: Automatic detection of ships in RADARSAT-1 SAR imagery. *Can. J. Remote Sens.,* **27**, 568–577.

Watson, C., R. D. Chapman, and J. R. Apel, 1992: Measurements of the internal wave wake of a ship in a highly stratified sea loch. *J. Geophys. Res*., **97** (C6), 9689–9703.

Yeremy, M., G. Geling, M. Rey, B. Plance, and M. Henschel, 2002: Results from the Crusade ship detection trial: polarimetric SAR. *Proc. 2002 Int. Geosciences and Remote Sensing Symp.*, Toronto, Canada, IEEE, Volume 2, pp. 711-713.